

WRF-Fire: Coupled Weather–Wildland Fire Modeling with the Weather Research and Forecasting Model

JANICE L. COEN,* MARQUES CAMERON,[#] JOHN MICHALAKES,[@] EDWARD G. PATTON,*
PHILIP J. RIGGAN,& AND KARA M. YEDINAK**

* National Center for Atmospheric Research,⁺ Boulder, Colorado
[#] Woodbridge, Virginia

[@] National Renewable Energy Laboratory, Golden, Colorado

& U.S. Department of Agriculture Forest Service Pacific Southwest Research Station, Riverside, California
** Department of Civil and Environmental Engineering, Washington State University, Pullman, Washington

(Manuscript received 30 January 2012, in final form 30 July 2012)

ABSTRACT

A wildland fire-behavior module, named WRF-Fire, was integrated into the Weather Research and Forecasting (WRF) public domain numerical weather prediction model. The fire module is a surface fire-behavior model that is two-way coupled with the atmospheric model. Near-surface winds from the atmospheric model are interpolated to a finer fire grid and are used, with fuel properties and local terrain gradients, to determine the fire's spread rate and direction. Fuel consumption releases sensible and latent heat fluxes into the atmospheric model's lowest layers, driving boundary layer circulations. The atmospheric model, configured in turbulence-resolving large-eddy-simulation mode, was used to explore the sensitivity of simulated fire characteristics such as perimeter shape, fire intensity, and spread rate to external factors known to influence fires, such as fuel characteristics and wind speed, and to explain how these external parameters affect the overall fire properties. Through the use of theoretical environmental vertical profiles, a suite of experiments using conditions typical of the daytime convective boundary layer was conducted in which these external parameters were varied around a control experiment. Results showed that simulated fires evolved into the expected bowed shape because of fire-atmosphere feedbacks that control airflow in and near fires. The coupled model reproduced expected differences in fire shapes and heading-region fire intensity among grass, shrub, and forest-litter fuel types; reproduced the expected narrow, rapid spread in higher wind speeds; and reproduced the moderate inhibition of fire spread in higher fuel moistures. The effects of fuel load were more complex: higher fuel loads increased the heat flux and fire-plume strength and thus the inferred fire effects but had limited impact on spread rate.

1. Introduction

Wildland fire modeling describes a broad range of approaches aimed at understanding and anticipating fire behavior—the way in which a fire ignites, develops, and spreads, and phenomena arising from it—as well as secondary fire effects. Fire behavior includes the rate at which the flaming front (the interface between burning

and unburned fuel) advances, the heat-release rate (which is related to the burning intensity), and phenomena such as the bowing forward of the flaming front, the transition from surface to crown fires, and extreme fire activity such as fire whirls. Fire effects include ecological and hydrological effects on the landscape, such as the percentage of forest fuel consumed in prescribed fires, tree mortality, and soil impacts, and air-quality impacts such as the emission rate, components, and cumulative quantity of smoke produced. Here, we introduce and apply a modeling tool that couples a numerical weather prediction (NWP) model with a wildland fire-behavior module that represents the growth of a fire propagating through surface fuels. It is hypothesized that, by using a few semiempirical relationships to parameterize physical processes of a fire that are not resolvable at

⁺ The National Center for Atmospheric Research is sponsored by the National Science Foundation.

Corresponding author address: Janice L. Coen, National Center for Atmospheric Research, P.O. Box 3000, Boulder, CO 80301.
E-mail: janicec@ucar.edu

atmospheric-modeling grid scales, commonly observed wildland fire behavior including the documented differences among fires evolving in different environmental conditions will naturally result. This occurs through interactions of physical processes in the simulations—to be specific, the dynamical exchange of forces between the fire and its atmospheric environment (“fire–atmosphere interactions”).

Firefighter training materials (National Wildfire Coordinating Group 1994) have historically taught that three external environmental factors affect wildland fires: weather, fuel characteristics, and topography. These are still the primary parameter inputs to a wide range of surface fire-behavior models. Fuel factors include the fuel type; the mass loading per unit area; physical characteristics of composite fuel beds such as the particle sizes, depth, and packing density; and time-varying characteristics such as live and dead fuel moisture. Topographic factors emphasize the terrain slope but also include orientation toward the sun; barriers that can interrupt the fire spread such as creeks, roads, and unburnable fuel; and topographic arrangements that lead to airflow effects such as narrow canyons. Of the three external factors, the most rapidly changing is weather (primarily fields such as wind, temperature, relative humidity, and precipitation). Wind changes, brought by phenomena such as fronts, downslope windstorms, convective downdrafts, sea and land breezes, and diurnal slope winds, can be particularly important because they can suddenly change the fire’s direction and behavior.

This core knowledge is evolving. Although fire-behavior models such as BehavePlus (Andrews et al. 2008) and Fire Area Simulator (FARSITE; Finney 1998) treat the three environmental factors as independent influences, they are not. Weather affects wildfires through fuel and terrain by controlling the fuel moisture through precipitation, ambient relative humidity, and increased evaporation driven by winds and by complicating the fire-spread-accelerating effect of steep slopes with topographically induced accelerations. Weather and terrain combine to produce distinctive topographic airflow regimes. Fuel properties vary with topography because plant productivity varies with elevation or with the aspect with respect to the sun. Fuel properties respond to local precipitation and temperature variations with high spatial variability. Moreover, it has long been recognized that fires “create their own weather.” That is, the heat and moisture created by the fire feed back into the atmosphere, creating intense winds that drive the fire’s behavior, sometimes overwhelming the effect of ambient winds. This evolving picture of the complexity and interaction of the forces shaping fires has been introduced into numerical models. In their presentation of

coupled models of cloud-scale NWP and wildland fire behavior, Clark et al. (2004) showed that simulated fires reproduced basic aspects of fire behavior such as the evolution of the “universal fire shape” (Albini 1993). This naturally occurring bowed shape of a fire front expanding in uniform, constant winds, is composed of a heading region (the fastest-spreading, highest-intensity leading edge), the flanks along each side where winds are shaped by the fire to be parallel to the fire, and the low-intensity backing region that creeps slowly against the wind.

Three fundamental concepts widespread within atmospheric science are emerging as central to further progress in wildland fire science. First, in contrast with the hypothesis that surface weather stations and diagnostic surface wind models sufficiently indicate the winds driving a nearby fire (e.g., Potter and Butler 2009), the complex time- and space-varying nature of weather has an important, perhaps dominant, impact on the evolution of a wildland fire. For example, simulations (Coen and Riggan 2010) using the Coupled Atmosphere–Wildland Fire–Environment (CAWFE) model showed that during the Esperanza Santa Ana–driven wildfire complex, transient, three-dimensional atmospheric channeling and wave dynamics generated by mountains and small-scale topographic lee effects caused strong near-surface gusty winds that drove the fire rapidly to the west-southwest, even though the closest surface stations recorded easterlies. This suggests an important role for wildland fire models that incorporate a full NWP model to simulate three-dimensional, time-varying weather and impacts on the fire.

Second, dynamic models, that is, models that calculate the forces causing motion (in contrast to kinematic models that calculate rate of motion without regard to the forces causing it), are necessary to represent the exchange of forces between the atmosphere and fire (Coen 2011) and to uncover the physical basis for fire phenomena. Kinematic models, which are the most prevalent type used in wildland fire modeling [e.g., FARSITE (Finney 1998), BehavePlus (Andrews et al. 2008), and Prometheus (Tymstra et al. 2010)], have been widely applied in estimating rates of spread of fires in various terrain, fuel, and wind conditions—in particular, when quick estimates are needed in field applications. Their limitations appear in attempts to apply them beyond estimates of the rate of spread to anticipate changes of behavior arising from fire-generated winds, dynamic interactions such as blowups, interactions between multiple fires, and fire phenomena such as fire whirls. For these issues that involve the exchange of forces between the fire and the atmosphere, dynamic models are required. By isolating the fire’s effects on the

atmospheric environment, a previous study (Coen 2005) showed that the fire's impact on the ambient wind velocity can be as great as several meters per second even 5 km away, can create on the order of 10° of buoyancy near the surface, and, in the case of large fires, can possibly become the dominant weather event in its vicinity.

A third factor not widely recognized in wildland fire science is that, although all computational fluid dynamics (CFD) models attempt to represent the fluid-dynamics exchange of forces with and heat transfer from wildland fires, the scale at which the equations are closed and the parameterizations used in closing the equations differ widely across CFD model type. NWP models are a subset of CFD models that are designed to capture the processes controlling weather patterns at scales ranging from continental scales (i.e., thousands of kilometers) down to local topographic scales (on the order of 10 m). Their attributes influencing winds and fire behavior include the initial background atmospheric state, thermodynamic heating and accelerations arising from vertical motions in a stratified atmosphere, the effect of terrain on airflow, calculation across several orders of magnitude in spatial scales frequently employing nesting of grids for spatial refinement, cloud-physics processes and the thermodynamic effects of phase changes on atmospheric motions, and extensive representation of atmospheric coupling with surface properties and processes in the atmospheric boundary and surface layers. Thus, we distinguish between two types of CFD models that are both referred to as coupled atmospheric–fire models: 1) those that typically simulate fluid flow in small domains (i.e., less than 1 km³) (e.g., Linn et al. 2002; Mell et al. 2007), neglecting some or all terrain effects, buoyancy effects from vertical motions in a stratified atmosphere, and phase changes associated with cloud formation, and 2) those simulating fluid flow with NWP models that bring forth the influences on fire behavior of synoptic pressure gradients, atmospheric stratification, cloud forcing, frontal passages, complex terrain, diurnal variability, and land surface coupling. Examples of the latter include the models of Clark et al. (2004) and Coen (2005) and the model discussed here. Mandel et al. (2011) describe an intermediate software build of the Weather Research and Forecasting model (WRF) between version 3.2 (V3.2) and V3.3 (V3.3 was incomplete at the time of their submission) that they modified, for example, to include heuristic approximations for reduction of near-surface wind speeds and assumed relationships between land surface properties and fuel parameters; these approximations were not included in WRF V3.3. Their model does not include later V3.3 additions to the atmospheric component and fire module, corrections to programming implementations in the rate of spread, and

corrections to backing and zero-wind rates of spread. Mandel et al. (2011) gathered applications of the model, including an application to crown fires, where the surface fire-rate-of-spread algorithm predicts that fires will creep through forest litter such as needles, twigs, and fallen leaves. The need for dynamic models such as these that represent the evolving three-dimensional weather and the feedbacks with wildland fires motivates this work.

Evaluation of coupled atmosphere–fire models requires a combination of studies and complementary approaches, each of which has strengths and weaknesses. One approach is to compare simulations of individual wildland fire events with measurements. No datasets complete enough to rigorously constrain and evaluate these more complex models exist, however—datasets collected before the past few years were designed with the models available at the time in mind, and, as a result, coupled models have been validated piecemeal, for example, by evaluating gross characteristics of simulated fires such as the rate of spread of the leading edge. For example, two historical datasets are presented by Cheney et al. (1993) and Cheney and Gould (1995). They collected fire-spread observations in hundreds of grass fires, relating fire rate of spread to ambient wind speed and fuel conditions. Cheney et al. (1993) presented time series of 2-m wind speeds and evolution of one fire's shape at 2-min intervals. Mell et al. 2007 used this fire to test simulations with a coupled atmosphere–fire model using several constant ambient wind speeds and various ignition line lengths but were limited to comparing the rate of spread of the leading edge and growth of the fire perimeter. Even in such simple experiments, the shifting wind speed and direction affected the evolution of the fire shape (Cheney and Gould 1995), and the ambient wind speeds measured concurrently at four corners of a plot varied from 3 to 6 m s⁻¹ with little apparent correlation. A more recent dataset (Clements et al. 2007) that was designed to study the structure of a flaming front captured measurements of winds and heat fluxes during the fire's passage, accompanied by nearby vertical profiles and surface weather stations recording time series of temperature, humidity, and wind. These measurements potentially enable modelers to evaluate model representations of internal feedback processes. [Mandel et al. (2011) compared simulated updrafts with those measured on an instrumented tower.] This dataset lacks the spatial maps of fire progression at frequent intervals that are required to validate two- or three-dimensional models, however. Moreover, in small experiments that are not dominated by strong mesoscale or synoptic forcing, small features in the terrain, land surface, fuel distribution, and atmosphere [e.g., the wind shifts in Cheney and Gould (1995), the atmospheric

structure from the recent frontal passage in Clements et al. (2007), and the structure of boundary layer turbulence] may all be of primary importance.

The lack of complete datasets is compounded in landscape-scale fires. Some notable attempts to produce datasets for evaluating a range of models have been made, including experimental burns such as the International Crown Fire Modeling Experiment (Alexander et al. 1998) and “FROSTFIRE” (Hinzman et al. 2003) in boreal forests and Project Flambeau (Palmer 1981), which demonstrated the generation of fire winds in a firestormlike experimental burn. Again, these are incomplete from the perspective of coupled atmosphere–fire models, contain periods of natural fire runs that last only minutes, and lack information on to where the fire has grown in short time intervals. As noted by Kremens et al. (2010), measurements must be commensurate with the scale of the phenomena—detailed ground-based measurements of radiant energy release such as those in Butler and Dickinson (2010) would not be representative in large fires because of the variability along a fire line (Riggan et al. 2010). Airborne infrared instrumentation such as FireMapper provides spatial maps of fire activity at frequent return intervals, but estimates of spread rate become challenging in landscape-scale fire data because flank runs and wind shifts make it difficult to connect point to point how far a fire spread (and therefore what the rate of spread was) between passes. A landscape-scale case study makes it difficult to identify which of many atmospheric or fire-module parameters are affecting the simulation without prior sensitivity tests such as we present here. In addition, the purpose of using coupled models goes far beyond simulating the rate of spread of the leading edge of the fire or the growth of the fire’s perimeter under fixed assumptions about the fire-line shape. Although coupled models produce those things, a much broader purpose is to explain fire phenomena, many of which have been photographed but not reproduced in experimental fires.

Another limitation of this approach—the comparison of a model simulation with measurements from a single event—and an issue with weather modeling in general is that, because of the limits of predictability, specific details of events—in particular, finescale features—are not predictable. One may anticipate that a “good” model, initialized with a range of initial conditions, will produce an envelope of solutions that gives guidance about the overall character of an event (M. Weisman 2012, personal communication), however. Such sensitivity experiments are another way to validate a model by showing that simulated and real systems respond in the same overall way. This understanding of the value of the sensitivity of a model’s response already guides the use of FARSITE

in field applications, where, using a wind measurement, users calibrate the fuel load to get the observed spread rate and then use the adjusted fuel load to forecast the next burning period’s rate of spread.

The purpose and scope of the current work is to present a coupled atmosphere–wildland fire model that is based on the WRF NWP model coupled to a wildland fire module called WRF-Fire that is composed of a subset of physical processes from the CAWFE model. In this work, we apply it in idealized simulations as an initial evaluation of modeled fire behavior’s sensitivity to environmental factors. These simulations are run in a turbulence-resolving large-eddy-simulation (LES) mode in which the fire is initiated into fully developed boundary layer turbulence generated through interactions with the land surface (i.e., through loss of momentum and a specified ground heat source) to allow for dynamic interactions between the fire-generated winds and coherent atmospheric turbulent motions. The methods section describes the composition of the coupled weather–fire model. The experiment-design section describes how this model is applied in a suite of experiments in which fundamental parameters known to influence fire behavior are varied. The validation issues we have presented have shaped our approach, which is to examine the sensitivity of our modeling system to a range of several environmental parameters that span the environmental conditions for one common type of fire, small fires ignited in the daytime convective boundary layer. By discussing how and to what degree each parameter influences the overall properties of a simple fire, this approach provides a foundation for future studies. Parameters such as wind speed have been tested before by coupled models, although not with shear-generated and convectively generated turbulence, whereas other parameters presented here have not. We have, where available, used measurements, none of which would be complete enough on its own to constrain and evaluate this model, and previous modeling studies with related models to frame these results. We use previous modeling studies because some knowledge about fire behavior arises only from modeling studies, such as understanding of phenomena seen in photos but not reproduced in laboratory, experimental, or fortuitously captured wildfires. The results section presents the outcome of the sensitivity experiments; these results are distilled in the conclusions. The discussion section presents thoughts on the broader use of the model and the study’s broader significance. This work is only one step toward assessing its abilities. Because WRF with the physics module WRF-Fire included can be applied at spatial scales ranging from small fires in large-eddy simulations of the planetary boundary layer at a horizontal grid spacing of

tens of meters to landscape-scale mesoscale fire simulations on the order of 1–10-km grid spacing, no one approach or study is sufficient to evaluate it.

2. Methods

a. Description of coupled weather–fire modeling system

WRF-Fire is a wildland fire physics module within the WRF model that allows explicit treatment of the effects of fire on atmospheric dynamics and feedback to fire behavior; thus the simulated fire can “create its own weather.” The fire component describes fire behavior in surface fuels and is fully coupled with the weather model so that exchanges between the two components occur at each time step throughout the simulation. The simulated atmosphere exerts a force in the form of wind on fires, directing where and how fast they spread. Local near-surface winds from the atmospheric model are passed to the fire module and, along with fuel conditions and local topography gradients, are used to determine a fire’s instantaneous spread rate and direction. Meanwhile, simulated fires consume fuel composed of live and dead vegetation and release heat and water vapor into the air, causing it to rise; the confluence of winds into this plume changes the winds in the fire’s environment. The fire module calculates the fuel consumed and thus the energy released by the fire and returns this information to the atmospheric component, where the energy is released as sensible and latent heat in the lowest layers of the atmospheric model. Other links between the two components are possible, for example, through fuel moisture dependence on weather, but are not yet included. Both components are described next.

b. Atmospheric model component

The WRF model (Skamarock et al. 2005) is a community mesoscale NWP model designed to be a flexible, state-of-the-art tool that is portable and computationally efficient on a wide variety of platforms. Formulated in a fully compressible and nonhydrostatic manner, WRF solves a set of equations of fluid motion, mass conservation, and atmospheric thermodynamics and predictive equations for several water states to produce a forecast of air velocity, temperature, water vapor, cloud water, rain, and ice concentrations on a three-dimensional grid. On this grid, variables are located in an Arakawa-C arrangement in a terrain-following hydrostatic-pressure vertical coordinate system. Nesting capabilities allow users to simulate weather over a large region while inner domains model flow at higher spatial and temporal resolution over a subset of the region. It

therefore is able to represent the three-dimensional, time-varying atmospheric structures such as atmospheric fronts, windstorms, downslope winds, cloud convective updrafts, and outflows that may affect fire behavior. WRF’s ability to capture many bulk characteristics of the daytime turbulent atmospheric boundary layer has been previously established (e.g., Moeng et al. 2007).

c. Wildland fire-behavior component

WRF-Fire is a physics module in WRF (see online at <http://www.wrf-model.org>), available in releases 3.2 (April of 2010) and later, that allows users to simulate the growth, propagation, and decay of wildland fires. It is similar to and can supplement other physics modules such as land surface models in that it treats interactions and exchanges between processes on the two-dimensional land surface and in the three-dimensional atmosphere. The spread of and heat release from a wildland fire propagating through fuels such as grass, shrubs, and vegetation litter are represented in a two-dimensional layer at the earth’s surface. The physical processes in WRF-Fire are a subset of the algorithms implemented by Clark et al. (2004) and Coen (2005), but in WRF-Fire the capabilities of the module are currently limited to a surface fire, that is, a fire spreading through fuels lying on the surface, grass, or shrubs. Crown fires (fires that spread into and through the canopies of trees) are not treated. Patton and Coen (2004) introduced the implementation of a fire behavior module in WRF. Yedinak et al. (2010) described some sensitivity studies of prescribed fires to ignition parameters and atmospheric stability. We describe WRF V3.2 and use it, with corrections to several errors at the programming level and corrections as stated here to backing rates of spread that are included in V3.3 and later, in these experiments.

Three components treat physical processes (the rate of spread of the flaming front, postfrontal heat release, and upscaling of heat release into the atmospheric model) and an additional algorithm defines the subgrid-scale interface. A diagram of the components is given in Fig. 1. Because these components represent wildland fire physical processes that occur at scales much smaller than the atmospheric grid size and time step, the wildland fire module uses semiempirical relationships to parameterize subgrid-scale processes.

At the surface, each atmospheric grid cell is further divided into two-dimensional fuel cells (Fig. 2). The WRF software infrastructure allows the user to choose the refinement ratios in the two horizontal dimensions at run time. Most operations for regular arrays—input/output, interprocessor communication, and memory management—are supported for subgrid-refined arrays as well. In addition to wildland fire modeling, the WRF

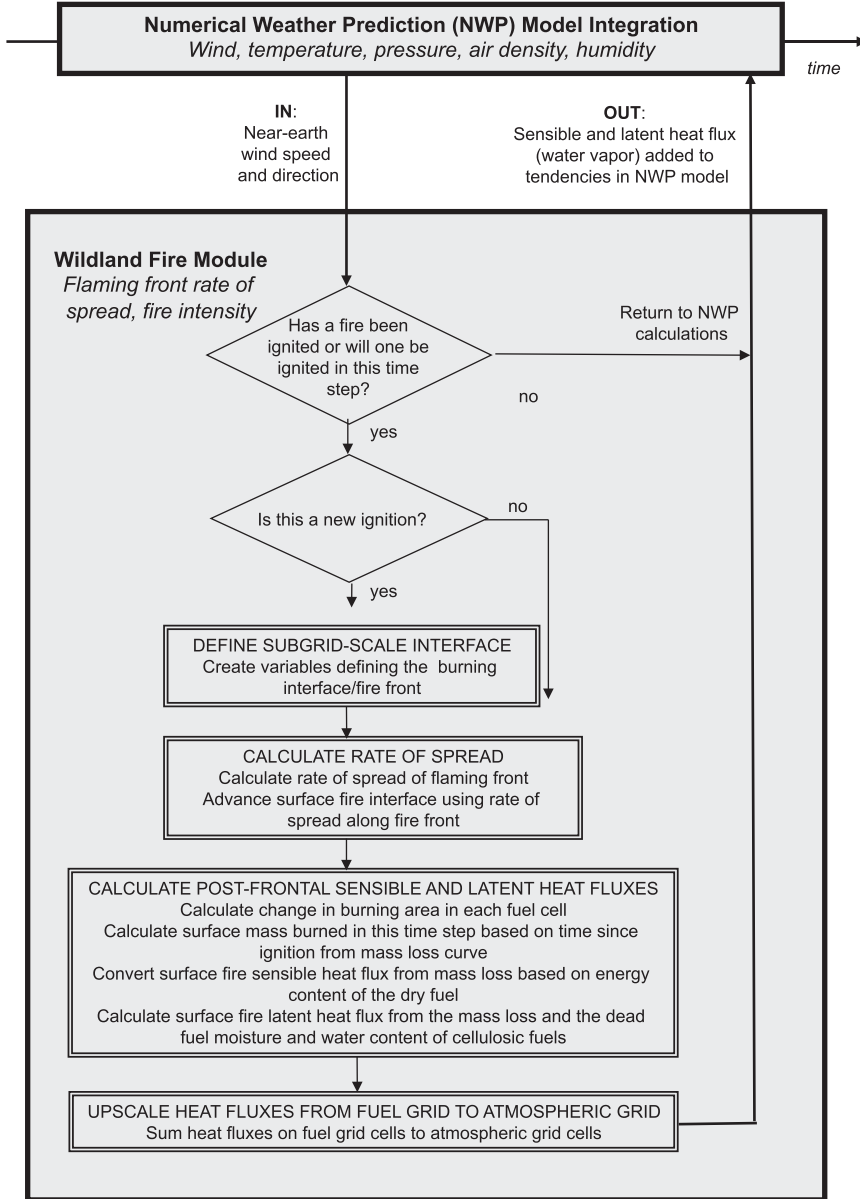


FIG. 1. The components of the WRF coupled weather–fire model.

subgrid-array capability is being used for binning schemes in atmospheric chemistry, land surface processes, and regional climate applications.

1) RATE OF SPREAD OF THE FLAMING FRONT

Local near-surface winds from the atmospheric model are interpolated to the fire grid and used, with fuel conditions and local topography gradients, to determine the speed with which (the “rate of spread”) and direction in which the fire spreads into areas of unignited fuel. Fire spread rates are calculated at points within

each fire grid cell as a function of fuel properties, the wind component normal to the fire line (which includes the fire’s effects), and terrain slope using the point-based algorithm of Rothermel (1972) at points along the fire line. This algorithm relates the rate of spread of the flaming front to local wind, terrain slope, and a set of fuel characteristics for each fuel type. By using calibration terms to relate its theoretically based core to actual fires, it aims to capture the effect of all processes that propagate the fire, including radiation heating, drying, and igniting unburned fuel; convective heating; contact ignition;

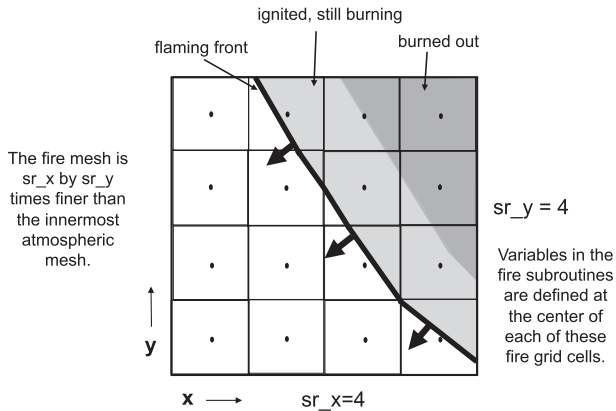


FIG. 2. Within each x - y atmospheric grid cell on the earth's surface is a further refined (sr_x in x and sr_y in y) mesh of fire grid cells. In this image, the fire mesh is 4 times as fine in both directions as the innermost atmospheric mesh.

and the spotting of small flaming embers short distances ahead of the fire line without representing each process, as shown in Eq. (1):

$$R = R_o(1 + \phi_s + \phi_w). \quad (1)$$

This equation, developed for fuel complexes in the United States, is semiempirical: the rate of spread of the leading edge of the flaming front R (m s^{-1}) is related to an expected no-wind rate of spread R_o that is a function of fuel properties only for still ambient air on level ground. Rothermel (1972) empirically determined functions of terrain slope ϕ_s (dimensionless) and wind speed ϕ_w (dimensionless) using small flame experiments on varying slopes in a wind tunnel and McArthur's (1969) grass-fire data in varying wind speeds. Each of these terms is a function of other properties; we refer the reader to the appendix in Rothermel (1972) for details. We repeat here only what is needed for discussion or is calculated or applied in a different way from the original.

The term R_o is calculated as

$$R_o = \frac{I_R \xi}{\rho_b \varepsilon Q_{ig}}, \quad (2)$$

in which I_R is the reaction intensity (W m^{-2}) characterizing the rate of heat release per unit area per unit time in the fire; ξ is the propagating flux ratio (dimensionless); ρ_b is the oven dry bulk density (kg m^{-3}), that is, the mass of fuel per cubic meter of fuel bed; ε is the effective heating number (dimensionless), that is, the fraction of the fuel that initially must be elevated to ignition temperature; and Q_{ig} is the heat of preignition (J kg^{-1}), that is, the amount of heat required to heat 1 kg of fuel to combustion temperature. Equation (2)

can be interpreted thus: the rate of spread is related to the ratio of the amount of heat received by the fuels ahead of the flaming zone (the numerator) tempered by the amount of heat it takes to raise the fuel to combustion temperatures (the denominator).

The wind coefficient ϕ_w is calculated following Rothermel (1972):

$$\Phi_w = CS^B(\beta/\beta_{op})^{-E}, \quad (3)$$

where S is the magnitude of the component of the wind velocity normal to the fire line. The coefficients C , B , and E and the optimum packing ratio β_{op} are calculated as in Rothermel (1972) as functions of the surface area-to-volume ratio of the fuel complex, and the packing ratio β (dimensionless), which may be interpreted as the fraction of the fuel-bed volume that is occupied by fuel. When the component of wind normal to the fire line is into the fire, the backing rate of spread in these experiments is the zero-wind rate of spread; this will be reformulated in future versions. Our use of Eq. (1) differs from the source and its use in kinematic models in that in coupled weather–fire models, the wind driving the fire has been modified by feedbacks from the fire as a natural consequence of the laws of fluid dynamics. The original assumption of an ambient wind unmodified by the fire and selection of an ambient wind without regard for the spatial and temporal variability in the wind structure belie current knowledge of fluid dynamics.

From observations and experimental evidence that this relationship does not perform well in Southern California chaparral fuels (Riggan et al. 2010), where fire spread may require substantial ambient wind, an alternative relationship (Clark et al. 2004) is available:

$$R = 1.2974S^{1.41}. \quad (4)$$

When the component of wind normal to the fire line is into the fire, the backing rate of spread is set to zero, because live chaparral generally requires wind or steep terrain to maintain flame propagation.

An alternative relationship (Noble et al. 1980) is available, developed for Australasian fuel complexes:

$$R = 0.18 \exp(0.8424S). \quad (5)$$

When the component of wind normal to the fire line is into the fire, the backing rate of spread is 0.18 m s^{-1} .

As is commonly done, we assume that Eqs. (1), (4), or (5) can be applied at real fire scales within a wide range of conditions (wind speeds of $<30 \text{ m s}^{-1}$), although Eqs. (4) and (5) are not used in this work. In addition, R is capped at 6 m s^{-1} . This cap addresses an issue with

Eq. (1), because fire rates of spread do not increase indefinitely with increasing wind speed. This limit was not triggered in these simulations. We also assume that the propagation speed normal to the interface can be calculated at all points along the fire front using Eqs. (1), (4), or (5), local fuel properties, and modeled winds and the local terrain slope, both normal to the fire line.

Equations (1), (4), and (5) require the velocity of the wind that, in principle, is driving the fire. This need presents a conceptual problem. As originally conceived in Rothermel (1972), a “midflame” wind speed represented the effect of the wind, where stronger winds tilted the flames toward the surface, increasing heat transfer and the fire’s spread. In light of understanding from atmospheric science that the winds over a strong heat source tend to be predominantly upward, the horizontal wind speed approaches zero at this confluence of winds into the updraft over the fire. Observations in grass fires support the existence of such a convergence zone at the fire front (Clements et al. 2007). In extreme phenomena such as dynamic fingering in which the fire grows forward in bursts evolving from vorticity dynamics, described in a modeling study by Clark et al. (1996b), the wind structure over the fire may be more complex. In practice, field applications of the Rothermel rate-of-spread formula use what is assumed to be an ambient wind, sometimes from the nearest Remote Automated Weather Station, with a heuristic reduction of winds to an estimated midflame height. This also ignores the temporal and spatial variability of winds and the fire’s dramatic shaping of winds in its environment. In CAWFE (Coen 2005), the user chooses a distance behind the fire line (upwind of the fire) and a height to which winds are interpolated, the default being the height of the fuel bed. This issue remains open but is unavoidable considering the extreme sensitivity of the predicted fire behavior to this parameter. Here, the latitudinal and meridional winds on WRF’s Arakawa C grid are located on the midpoints on the east and north sides, respectively, of the atmospheric grid cells. For these calculations, horizontal wind components from the two lowest above-ground model layers are averaged vertically and then horizontally interpolated to the center of the subgrid-scale fuel cells. The mechanisms through which wind affects a fire’s rate of spread and therefore how it should be incorporated in models remain an active area of research.

2) FLAMING-FRONT REPRESENTATION AND TRACKING

A common challenge in geophysical science models is how to represent a moving interface that is a result of complex subgrid-scale nonlinear internal dynamics. In WRF-Fire, the interface between the burning or burned

area and the unburned fuel is tracked using the level-set-method numerical technique introduced by Osher and Sethian (1988) with a detailed review in Sethian (1996). It was applied to wildland fire-front propagation in Mallet et al. (2009) and Rehm and McDermott (2009); Mandel et al. (2009) describe its implementation in WRF-Fire. The fire front advances normal to the front at a speed given by Eqs. (1), (4), or (5), but in this level-set approach a scalar function is given at nodes of the fire grid and the speed of the front is related to the gradient of the scalar function across the interface.

3) POSTFRONTAL HEAT RELEASE

A semiempirical algorithm (Clark et al. 2004) calculates the postfrontal heat-release rate that characterizes how rapidly the fire consumes fuels of different sizes with time after ignition, distinguishing between rapidly consumed grasses and slowly burned logs and other large fuel components. This algorithm assumes an exponential depletion of fuel mass from the time of ignition, calibrated for various fuel types burned in laboratory fuel-consumption experiments (Albini 1994; Albini et al. 1995). The fuel-consumption rate is controlled with a weighting parameter W that increases with particle size and characterizes the time (s) required for the fuel load (the mass of fuel per unit area) to decrease to a factor of e^{-1} of the original load:

$$1 - F(t) = \exp(-t/W), \quad (6)$$

where F is the fraction of fuel that has been burned and t is the time since ignition. The fire stops releasing heat when the fuel remaining approaches an infinitesimally small amount or the fuel moisture exceeds that fuel category’s moisture content of extinction.

4) PARTITION INTO SENSIBLE AND LATENT HEAT FLUX

Fuel consumption releases heat and water vapor. In the model, this release is partitioned into sensible and latent heat fluxes that contribute to the potential temperature and water vapor mixing ratio, respectively. The sensible heat flux H_s released by the ground fire is calculated as

$$H_s = \frac{\Delta M}{\Delta t} (1 - B) h_c, \quad (7)$$

where ΔM is the change in fuel mass in the current time step Δt , h_c is the heat of combustion (J kg^{-1}) for dry cellulose fuels, and B is the fraction of the total fuel mass that is water. The term B is related to the more commonly measured dead fuel moisture content M_f (the mass of water per unit mass of dry fuel) by

$$B = \frac{M_f}{1 + M_f}. \quad (8)$$

The latent heat flux LE_s released by the surface fire is calculated as

$$LE_s = \frac{\Delta M}{\Delta t} [B + 0.56(1 - B)] L_v, \quad (9)$$

where L_v is the latent heat of vaporization of water (J kg^{-1}). The first term arises from the water absorbed by the fuel from its environment and held between the cellulose cells of wood, and the second term accounts for the water bound in the cellulose fuel cells themselves, assuming 56% of the wood mass is water.

5) UPSCALING TO THE ATMOSPHERIC MODEL

The two-dimensional sensible and latent heat fluxes produced by the fire are summed from fire grid cells to the atmospheric cells in which they lie. These fluxes are returned to the NWP model where they are distributed vertically through an empirically estimated extinction depth. The extinction-depth concept (Clark et al. 1996a,b) is based on the assumption that a simple radiation treatment could be used to distribute the sensible and latent heat and smoke into the lowest atmospheric grid levels. That assumption was later supported by experimental results showing that the e -folding height over which the heat is distributed in the atmospheric model is typically 10 m for grass fires, from data in Clements et al. (2007), and 50 m for crown fires, from analysis of infrared observations of wildfires (Coen et al. 2004). The vertical flux divergences become additional tendencies to the potential temperature and water vapor prognostic equations, altering the atmospheric state.

6) IMPLEMENTATION

In each time step, the fire front—the interface between burning and nonburning fuel—is advanced, igniting fresh fuel while previously ignited areas continue to consume more fuel. The model can run on a relatively coarse grid, with the mesh size dictated only by desired resolution in the fire region and limitations imposed by terrain in the atmospheric model. Note that, unlike a combustion model, the fuel or fire temperature, the fire intensity, and the consumption rate of oxygen or flammable pyrolyzed gases are not variables that are tracked by this model, whereas the heat-release rate is a function of the time from ignition, the fuel properties, and the atmospheric state.

We note that the fire component cannot realistically be run separately without two-way dynamic coupling to the atmospheric component. Models without coupling

(such as FARSITE) must impose an additional constraint, a shape to points along the fire line, because otherwise a line ignition, experiencing the same wind along its length, would spread simply in a line, which is not realistic. The coupling shapes the wind strongly near the fire line, producing winds that blow strongly forward at the head, parallel to the fire's flanks (neither increasing nor impeding the fire's spread), and drawing winds into the fire across its backing region, impeding its growth. This dynamic constraint, evolving from the phenomena physics, results in a realistic fire shape. This effectively acts as a dynamic stability force—small perturbations along the flanks (resulting from fuel pockets, slope, or wind fluctuations) become fire whirls that travel downwind along the flanks toward the fire's head (Clark et al. 2004) while the winds along the flanks impede the flanks themselves from growing further. Large perturbations and wind responses that reinforce one another in the model may grow into dynamic instabilities, which are likely the basis for some extreme fire-behavior phenomena in natural fires.

3. Experiment design

a. Initialization

To initialize these experiments, atmospheric background states, terrain, and spatial distributions of fuel were specified, along with the number, time, and location of fire ignitions. In these theoretical experiments, an atmospheric profile of temperature was imposed within a 2-km-deep domain with constant potential temperature of 300 K in the lower 1 km and an overlying statically stable layer in the upper 1 km that increased linearly to 310 K at 2 km. The background water vapor mixing ratio was initially 0 kg kg^{-1} . The magnitude of the ambient horizontal wind was varied between experiments. The terrain in these experiments was flat. The standard method for characterizing fuel, that is, the live and dead vegetation available to burn, is to categorize it into “fuel models,” a standardized set of properties consisting of the mass loading per unit area, spatial distribution, and physical characteristics. Several categorization systems exist; here, the 13 fuel models identified by Albini (1976), restated with pictures by Anderson (1982), an industry standard, were used. Each experiment used a single horizontally homogeneous fuel model that varied among experiments.

b. Control experiment and suite of sensitivity experiments

The model was used to investigate the sensitivity of simulated fire characteristics such as perimeter shape,

TABLE 1. Experiments discussed in the text.

Expt name	Fuel model	Fuel load (kg m ⁻²)	Fuel moisture (%)	Wind speed (m s ⁻¹)	Surface area-to-volume ratio (m ⁻¹)	Packing ratio (dimensionless)
NoWind	1	0.167	5.50	0.00	11 483	1.07×10^{-3}
Control	1	0.167	5.50	2.50	11 483	1.07×10^{-3}
FCat3	3	0.674	5.50	2.50	4921	1.72×10^{-3}
FCat4	4	3.591	5.50	2.50	5705	3.83×10^{-3}
FCat5	5	0.784	5.50	2.50	5522	2.51×10^{-3}
FCat8	8	1.120	5.50	2.50	6198	3.58×10^{-2}
FCat10	10	2.692	5.50	2.50	5787	1.72×10^{-2}
LoadLo	1	0.083	5.50	2.50	11 483	1.07×10^{-3}
LoadHi	1	0.333	5.50	2.50	11 483	1.07×10^{-3}
WSLo	1	0.167	5.50	1.25	11 483	1.07×10^{-3}
WSHi	1	0.167	5.50	5.00	11 483	1.07×10^{-3}
FMLo	1	0.167	2.75	2.50	11 483	1.07×10^{-3}
FMHi	1	0.167	11.0	2.50	11 483	1.07×10^{-3}

the fire intensity, and rate of spread to external factors such as fuel characteristics and wind speed that are known to influence fires. Through the use of theoretical environmental vertical profiles, experiments were conducted in which external variables were varied around a control experiment. The suite of experiments varied the fuel category (among grass, shrub, and forest litter categories), the fuel loading (holding other fuel characteristics the same), the fuel moisture, and the ambient wind speed (Table 1). Among experiments, we compared the resulting perimeter shape, the rate of spread of the fire's head, the intensity of burning in the head, and the depth of the burning region.

For these experiments, WRF was configured in LES mode (Moeng et al. 2007), meaning that the grid, 40 m in the horizontal plane in these experiments, is fine enough to resolve the largest energy-containing motions responsible for turbulent energy transport while smaller-scale motions were parameterized by Deardorff's (1980) turbulent kinetic energy (TKE)-based subgrid-scale scheme. The turbulent boundary layer into which the fires ignite was driven by an imposed wind interacting with an idealized surface with an imposed sensible heat flux of 100 W m⁻² and a drag coefficient of 0.005, which corresponds to a roughness length of 0.03 m. These surface conditions, in conjunction with the range of wind speeds selected, are representative of a daytime convective boundary layer over grass plains or farmland (Arya 1988). The terrain slope could not be varied in this LES configuration because of the need to use periodic boundary conditions to establish a well-mixed boundary layer. The simulations initially ran for 0.5 h of simulated time to allow the boundary layer turbulence to develop and to equilibrate with the imposed forcing. The Smagorinsky and TKE coefficients were set to 0.18 and 0.10, respectively, as recommended by Moeng et al. (2007).

Next, a fire was ignited as a 40-m-wide, 1-km-long line in the *y* direction and was allowed to evolve during the remaining 2 h of each simulation.

The simulations used a single domain with atmospheric grid resolutions of 40 m in the *x* and *y* directions, with 51 stretched vertical levels between the surface and the model top at 2 km. The first three atmospheric vertical grid levels, converted from mass to estimated height, were located at 18.2, 54.6, and 91.2 m, with the first half-grid level (where horizontal wind components are located) at 9.1 m. The maximum vertical grid length was 43 m. The horizontal domain was 5 km in both directions. Periodic boundary conditions were used in the horizontal directions. At the surface, five by five subgrid fire cells lay within each atmospheric cell.

It is important to distinguish between predetermined outcomes and results arising from the model. For example, the use of Eqs. (1), (4), or (5) at points along the fire line predetermines that the fire will spread fastest where the wind speed is highest and, by Eq. (6), that fuels composed of larger fuel particles will release heat for longer times. In kinematic models that apply these relationships, this outcome would be predetermined and would simply follow from those equations. In these models, an additional constraint forces the flaming front in kinematic models to conform to a specific shape. For example, Richards (1990) and FARSITE (Finney 1998) used the Huygens wave-front principle to describe an expanding fire front as an ellipse. Other geometric shapes were surveyed by Tymstra et al. (2010). In all cases, the shape of the resultant fire line is predetermined. In contrast, in our dynamic coupled modeling framework, no such constraint on the shape of the flaming front is imposed. The two-way coupling between the atmospheric and wildland fire components provides a dynamic constraint that consistently shapes the atmospheric state (i.e.,

most directly the low-level winds, but also dynamically significant properties such as buoyancy, shear, and vorticity) in such a way that it in turn shapes the fire. Thus, the simulated fire shape is not predetermined but arises from the model physics.

4. Results

Although the rate of spread of the leading edge of the fire line is often of the most practical interest, we present the impacts on other fire characteristics—the fuel-consumption rate as shown in the magnitude of the sensible heat flux, the horizontal distance into the fire that is releasing heat (the “burning depth,” analogous to the flame depth), and the strength of the plume updraft—as they affect the outcome through the dynamics of a coupled model and discuss the implications for understanding wildland fire phenomena.

a. Simple no-wind case

We present a simple experiment—a fire spreading on flat terrain with no ambient wind other than the eddies of the well-mixed surface layer (experiment NoWind)—as context for understanding the impact of other environmental parameters on fire evolution in later experiments.

A 1-km-long fire line was ignited in short grass (as described by Anderson fuel model 1) after 0.5 h of simulation time. With no imposed wind, boundary layer turbulence developed because of the imposed buoyancy forcing; this regime is known in the boundary layer community as “free convection” (Schmidt and Schumann 1989). Typical wind speed fluctuations from the turbulent eddies were $2\text{--}3 \text{ m s}^{-1}$. At 0.5 h after ignition (Fig. 3a), the sensible heat flux, an indicator of how quickly fuel is being consumed and indicator of areas with the most intense burning, was weak and the winds were barely perturbed. The simulated fire grew slowly in all directions over the next 2 h (Figs. 3b–d). A convective column with peak updrafts of about 4 m s^{-1} at 700 m above ground level formed over the fire and drew air inward at its base, inhibiting fire growth by superimposing winds against the outward-directed fire propagation. As a result, the fire crept outward at an average rate of 0.02 m s^{-1} and produced very low peak sensible heat fluxes ($1\text{--}10 \text{ kW m}^{-2}$) with a narrow burning depth throughout the fire line. The slight variability in the fire line reflected the influence of the fluctuating horizontal wind components arising from turbulent boundary layer eddies that produced divergence or convergence at the surface that enhanced or discouraged outward fire growth, depending on their position relative to the fire line. The vertical velocity contours associated with these eddies (Fig. 4) developed the expected hexagonal cellular structure

known to characterize free-convective conditions (e.g., Schmidt and Schumann 1989).

b. Control experiment

In the control experiment, the fuel was short grass (fuel model 1) with a fuel moisture content of 5.5%, the terrain was flat, and an ambient wind of 2.5 m s^{-1} was imposed in the x direction. After a 0.5-h spinup for the turbulent boundary layer to develop, a 1-km-long fire line was ignited.

Over a 2-h period after ignition (Figs. 5a–d, 6a–d), the simulated fire evolved into the universal fire shape and maintained that shape as it grew, despite the presence of turbulent eddies, with a clearly defined, fast-spreading (0.22 m s^{-1}) head. The heading region was associated with the highest heat flux and was led by a convective plume. Winds blew parallel to the flanks toward the head. A low-intensity backing region crept slowly upwind. The burning depth was narrow and widest at the head of the fire, as has been observed in experimental fires in rapidly consumed grass fuels (Cheney et al. 1993). The spatial and temporal variability of the turbulent eddies added asymmetry, and variability in simulated properties compared qualitatively well to our own simulations without imposed turbulence (not shown) and those of others (e.g., Clark et al. 2004; Mell et al. 2007). Figures 5a–d show the three-dimensional structure and variability along the fire line that occurs in our simulations.

In contrast with the NoWind experiment, this experiment produced higher maximum sensible heat fluxes (approximately 25 kW m^{-2} ; Figs. 6a–d). Although conditions are not identical, these heat fluxes are similar to heat-flux measurements that have been made during burning in grass (Clements et al. 2007) or grass/litter mixes (Frankman 2009). In the simulation, areas with higher sensible heat fluxes revealed where the most rapid consumption of fuel occurred. This was consistently at the fire’s leading edge, where the fire-generated winds concentrated the heat released by the fire into a plume that drew winds underneath it and forward into fresh fuel, and was intermittently along the fire’s flanks, as eddies either enhanced the fire’s outward growth into unburned fuel or suppressed outward growth with wind components directed into the fire’s blackened interior where no fuel remained. Using higher-resolution simulations, Clark et al. (2004) found that such perturbations became fire whirls traveling forward along the flanks.

c. Sensitivity to fuel model and fuel load

1) FUEL MODEL

While intrinsic fuel properties such as the heat content, chemical degradation path, and particle density are

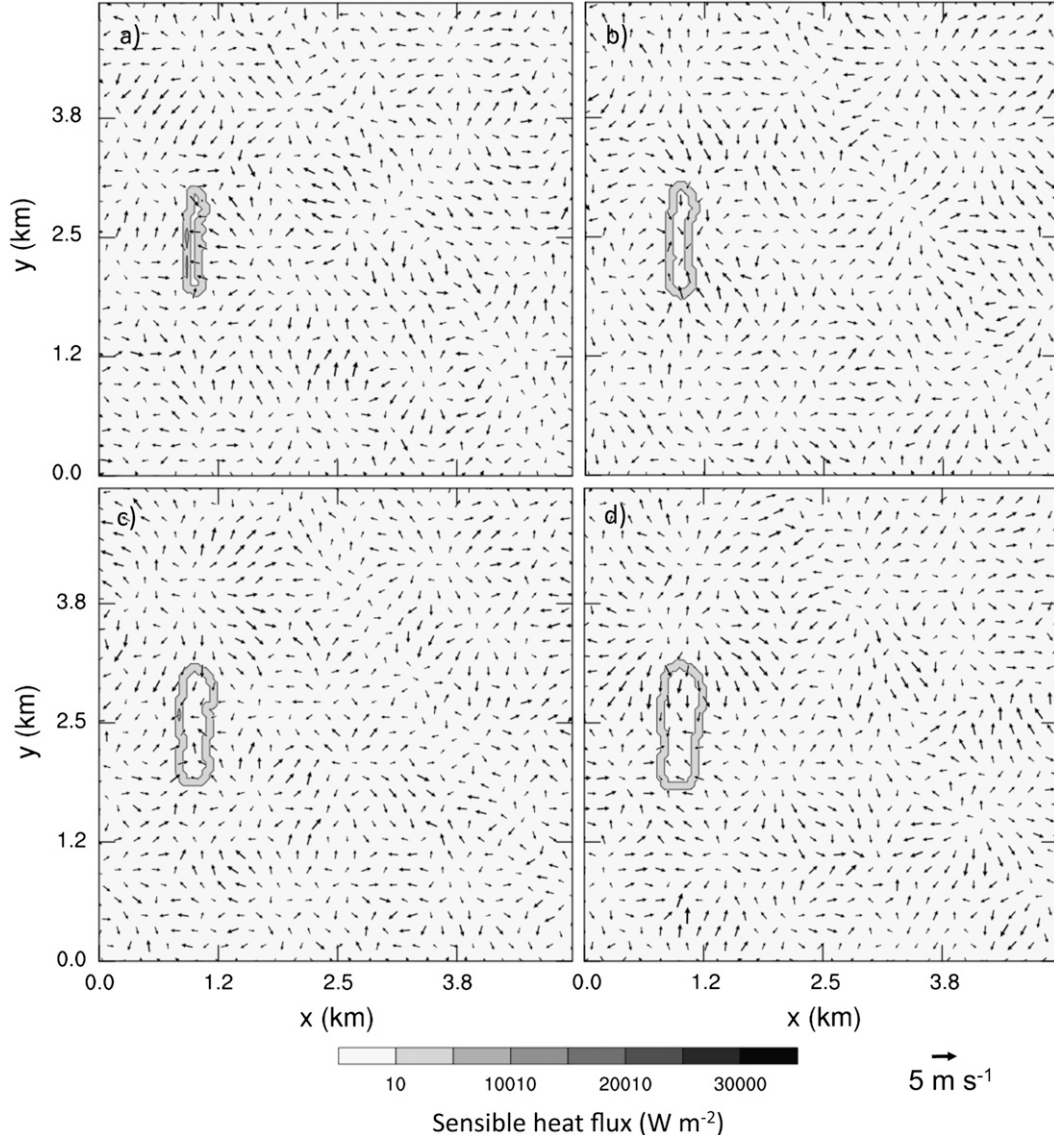


FIG. 3. Four time periods, (a) 1 h (0.5 h past ignition), (b) 1.5, (c) 2, and (d) 2.5 h, in the evolution of a fire in no-wind, no-slope conditions. Contours indicate sensible heat flux (W m^{-2}), and vectors indicate near-surface wind speeds at an elevation of 9.1 m.

of primary importance at the fundamental combustion scales, the Rothermel algorithm [Eqs. (1)–(3)] and associated fuel models determine fire behavior through the combined effects of several extrinsic fuel properties. These properties include fuel load (the mass of fuel per unit area), where a greater load is anticipated to increase the heat released by the fire; physical properties like surface area-to-volume ratio [denoted by σ (s^{-1})], where the higher σ of fine fuel particles allows faster fuel consumption; the packing ratio β for which low values would indicate widely spaced particles between which heat transfer is inefficient and high values represent

a tight packing of particles through which air cannot circulate; and the depth of the fuel bed. The different types of fire behavior expected with different intrinsic and extrinsic fuel properties are discussed in Pyne et al. (1996, chapters 1 and 3).

Here we simulated the evolution of fires in grass, shrub, and litter fuel types—short grass (fuel model 1, experiment Control; Fig. 7a), tall grass (fuel model 3, experiment FCat3; Fig. 7b), two shrub types including chaparral (fuel model 4, experiment FCat4; Fig. 7c) and brush (fuel model 5, experiment FCat5; Fig. 7d), and two forest litter categories, including closed-timber litter

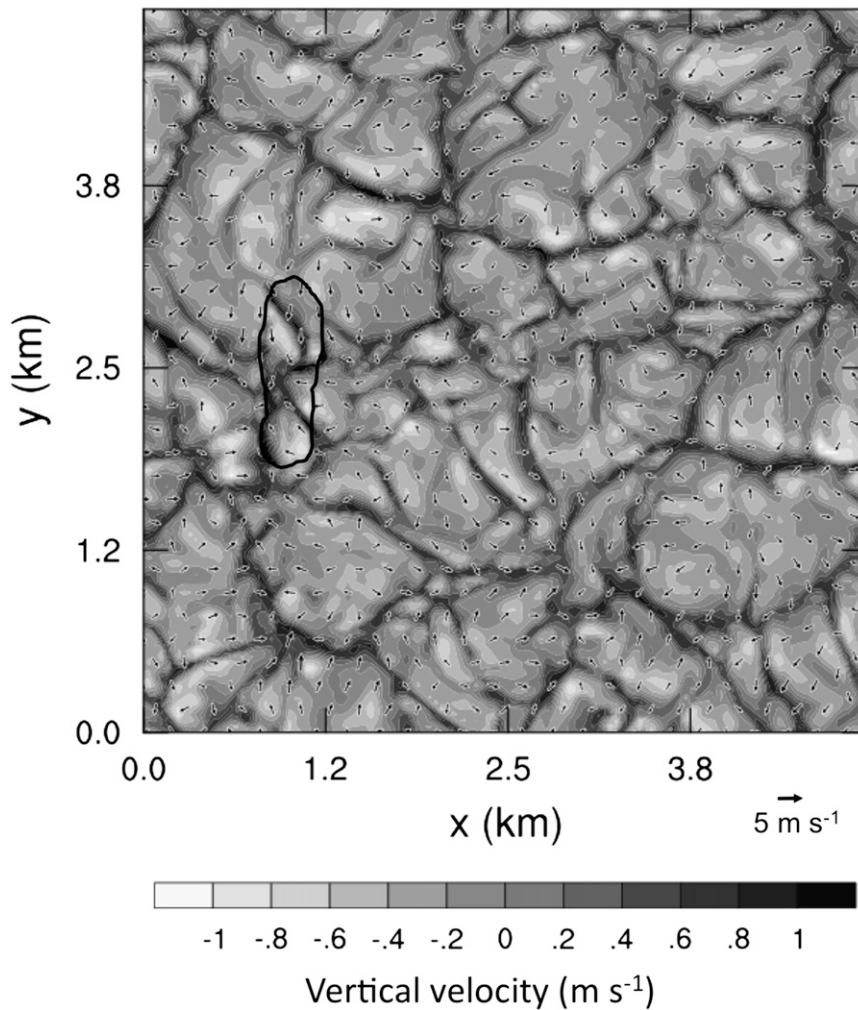


FIG. 4. The location of eddy updrafts and downdrafts and near-surface wind vectors with respect to the fire line at 2.5 h, the time of Fig. 3d. The vertical velocity at 18.2 m is shown by filled contours, corresponding to the grayshade bar at bottom, along with the horizontal velocity vectors at 9.1 m. The thick dark line indicates the outline of the fire.

(fuel model 8, experiment FCat8, also used as light loads of conifer forest litter; Fig. 7e) and timber litter along with an understory (fuel model 10, experiment FCat10, also used to represent heavy-timber litter; Fig. 7f). The coupled model reproduced well-known (e.g., Anderson 1982) differences in fire-line properties and head-fire intensity among three very different types of fuel: flash-burning grass fuel types (Figs. 7a,b), shrubs (Figs. 7c,d), and forest litter (Figs. 7d,e). Grass fuels, characterized by relatively low packing ratios and high porosity (prescribed in the fuel characteristics as a high value of σ), allow air to easily penetrate the fuel bed. In the model results, grass fuels quickly spread a narrow flame front with rapid fuel consumption and average velocity of 0.22 and 0.44 m s^{-1} for fuel models 1 and 3, respectively. Shrub fuel types had higher fuel loads containing some

larger fuel components and were represented by a lower average σ than grass. These fires consumed fuel and released heat over a 5–10-times-longer period, producing a fast-moving fire (0.20 and 0.33 m s^{-1} for fuel models 4 and 5, respectively) with substantial heat fluxes, depending on the specifics of the shrub fuel category. For example, FCat4 produced the highest heat fluxes of these experiments, approximately 50 kW m^{-2} . Forest-litter categories had fuel loads that were comparable to those of shrubs but had more mass distributed in larger fuel particles such as downed branches and logs and thus produced slow-moving fires (0.018 and 0.13 m s^{-1} for fuel models 8 and 10, respectively). Although they eventually released more heat (e.g., fuel model 8 has approximately 10 times the fuel load of fuel model 1), the heat release was distributed over the duration of the

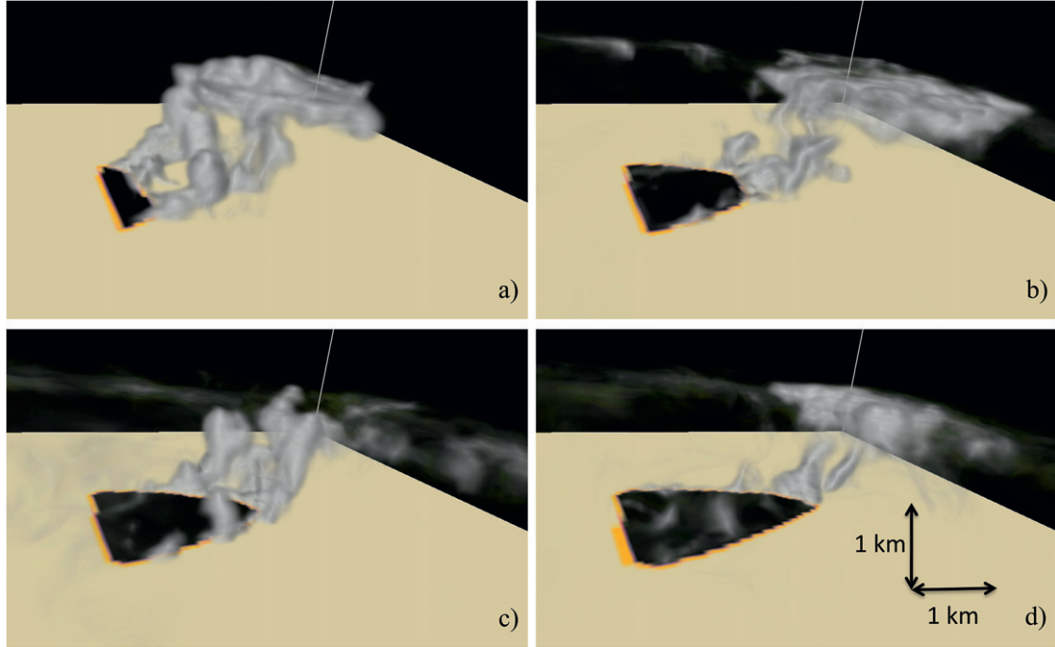


FIG. 5. A three-dimensional volume rendering of the water vapor field, used as a proxy for smoke at four time periods, (a) 0.75, (b) 1.25, (c) 1.75, and (d) 2.33 h, in the evolution of a fire in the control experiment. The orange field around the fire's blackened interior shows the sensible heat flux (W m^{-2}), which has a maximum of 25 kW m^{-2} .

simulation throughout the area of the fire and sensible heat fluxes were relatively low at 7 (FCat8) and 35 (FCat10) kW m^{-2} .

The simulated fires in tall-grass and shrub fuels varied from an elliptical shape (Fig. 7) depending on how they shaped the wind field. In particular, some experiments produced surface divergence (FCat3), stagnation zones (FCat10), and wind reversals (FCat4 and FCat5) in the horizontal winds immediately ahead of the fire. In some experiments, the winds over the head of the fire pass forward apparently unaffected by the fire (FCat8), whereas, in others, winds are shaped to travel along the front (FCat1, FCat3, and FCat10) or are drawn into the fire over the fire line (FCat4). The length of the fire line (1 km) was marginally long enough in a relatively weak wind to lead to the behavior described by Clark et al. (1996a), in which the fires could not sustain a single elongated convective updraft and broke up into multiple convective cells and accompanying convective fingers along the fire line. Linn and Cunningham (2005) produced this double-headed behavior while simulating 100-m-long grass fires in 1 m s^{-1} ambient winds but did not in shorter (10 m) fire lines or stronger winds, but they provided no explanation. A detailed analysis of the parameters leading to breakup of fire lines through this mechanism is not given here, although we observed it to occur in simulations (not shown) in which fire lines of at

least 1 km long burned at high heat-release rates along the length of the line in moderate ($3\text{--}4 \text{ m s}^{-1}$) winds.

2) FUEL LOAD

One of the variables that differentiated the fuel models in the previous section is the fuel load. An often-emphasized variable in practical applications, the fuel load is frequently presumed to be one of the, if not the, dominant fuel factors in fire behavior and fire effects. Van Wagner (1989) indicated that larger fuel loads could create larger spread rates by releasing more heat, accelerating the preheating of unburned fuels ahead of the fire line, and thereby increasing the spread rate. Rothermel's (1972) algorithm [as in Eq. (2)] posed the rate of spread as a ratio of a source term (the energy source propagating the fire) to a sink term (the energy sink required to raise potential fuel to the ignition temperature). Although the Rothermel formulation is widely used, a point often overlooked is that increasing the fuel load increases the source as well as the sink, and this limits the predicted impact of the fuel load on the rate of spread. Dupuy's (1995) work with laboratory experiments in pine-needle litter concluded that the rate of spread is proportional to the cube root of the fuel load. Cheney et al. (1993) concluded that fuel load did not influence fire spread in grassland fires. McAlpine (1995) found only a weak relationship between fuel consumption and the rate of

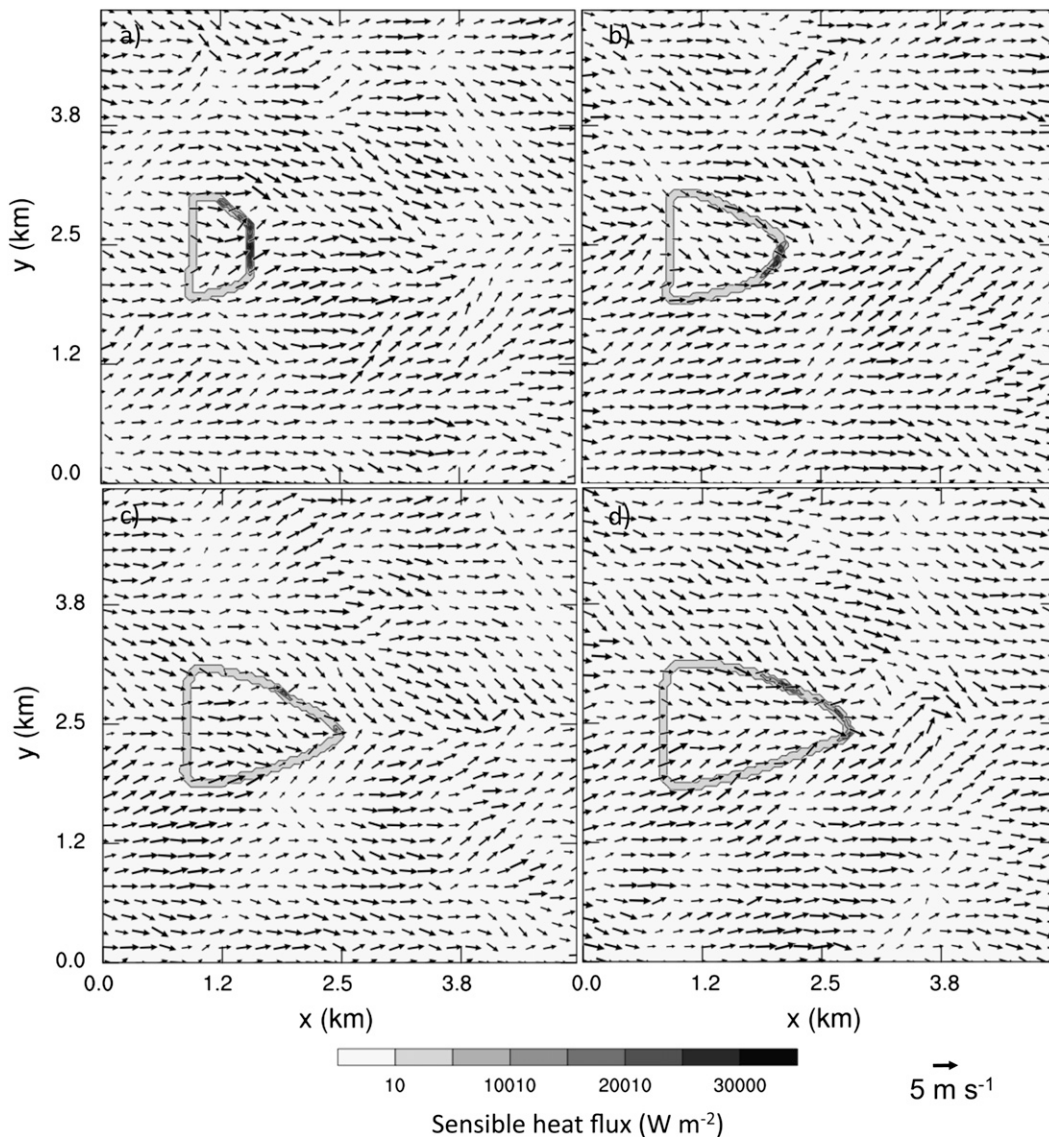


FIG. 6. Four time periods, (a) 1 h (0.5 h past ignition), (b) 1.5, (c) 2, and (d) 2.5 h, in the evolution of a fire in the control experiment. Contours show sensible heat flux (W m^{-2}), and vectors indicate near-surface wind speeds.

spread in his compilation of hundreds of experimental burns. Although these experimental studies do not indicate whether the fuel load affects other aspects of the fire and the circulation it creates, they do indicate a weak impact of fuel load on rate of spread, if any.

Here, we tested the sensitivity to fuel load by alternately doubling (experiment LoadHi) and halving (experiment LoadLo) the load of 0.167 kg m^{-2} used in the Control experiment (Figs. 8a–c). The effect of the doubled load was to increase the total heat released and the rate at which it was released to the atmosphere and to increase the fire plume's peak updraft over the fire (from $3.8 \text{ to } 10.0 \text{ m s}^{-1}$) as well as the horizontal motion of

replacement air into the plume's base. Decreasing the load produced converse effects on heat release and air motions, decreasing the plume's peak updraft (from $3.8 \text{ to } 3.5 \text{ m s}^{-1}$). Because horizontal winds decelerate as they are redirected up into the plume, however, near-fire horizontal winds determining the fire rate of spread could not vary in proportion to load across the experiments. Near-fire horizontal winds varied from $2 \text{ to } 4 \text{ m s}^{-1}$ in both Control and LoadLo and only accelerated to approximately 5 m s^{-1} in LoadHi. As a consequence, reducing the load by one-half reduced the forward rate of spread by one-fifth; doubling the load increased the spread rate by two-fifths.

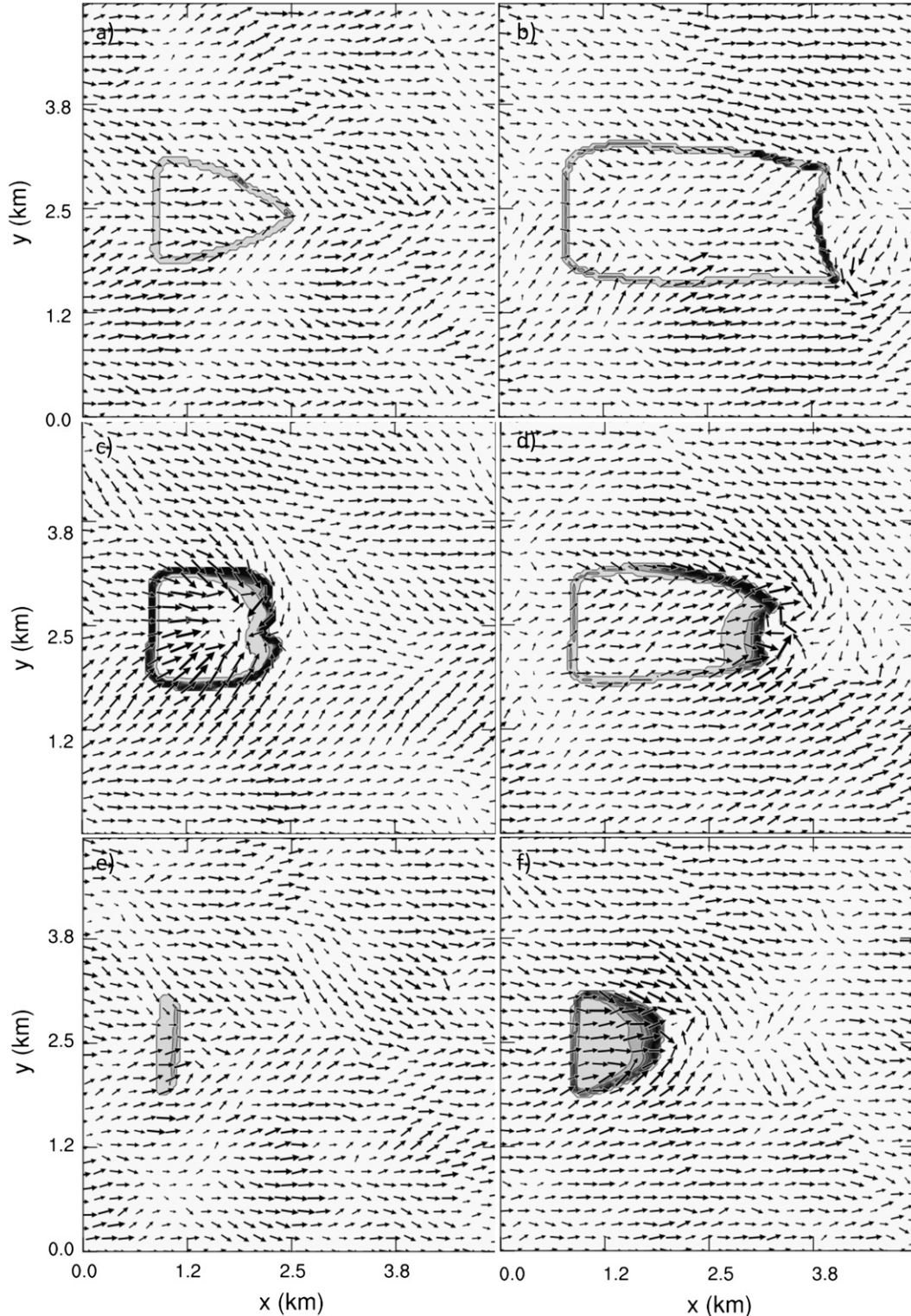


FIG. 7. Sensible heat flux (contours) and near-surface wind vectors at 2 h (1.5 h after ignition) for six simulations, each using a different fuel category: (a) fuel model 1, short grass; (b) fuel model 3, tall grass; (c) fuel model 4, chaparral (6 ft); (d) fuel model 5, brush (2 ft); (e) fuel model 8, closed-timber litter, also used to represent light-conifer litter; and (f) fuel model 10, timber litter and understory, also used to represent heavy-conifer litter. These use the same reference grayshade bar and vectors as in Fig. 6.

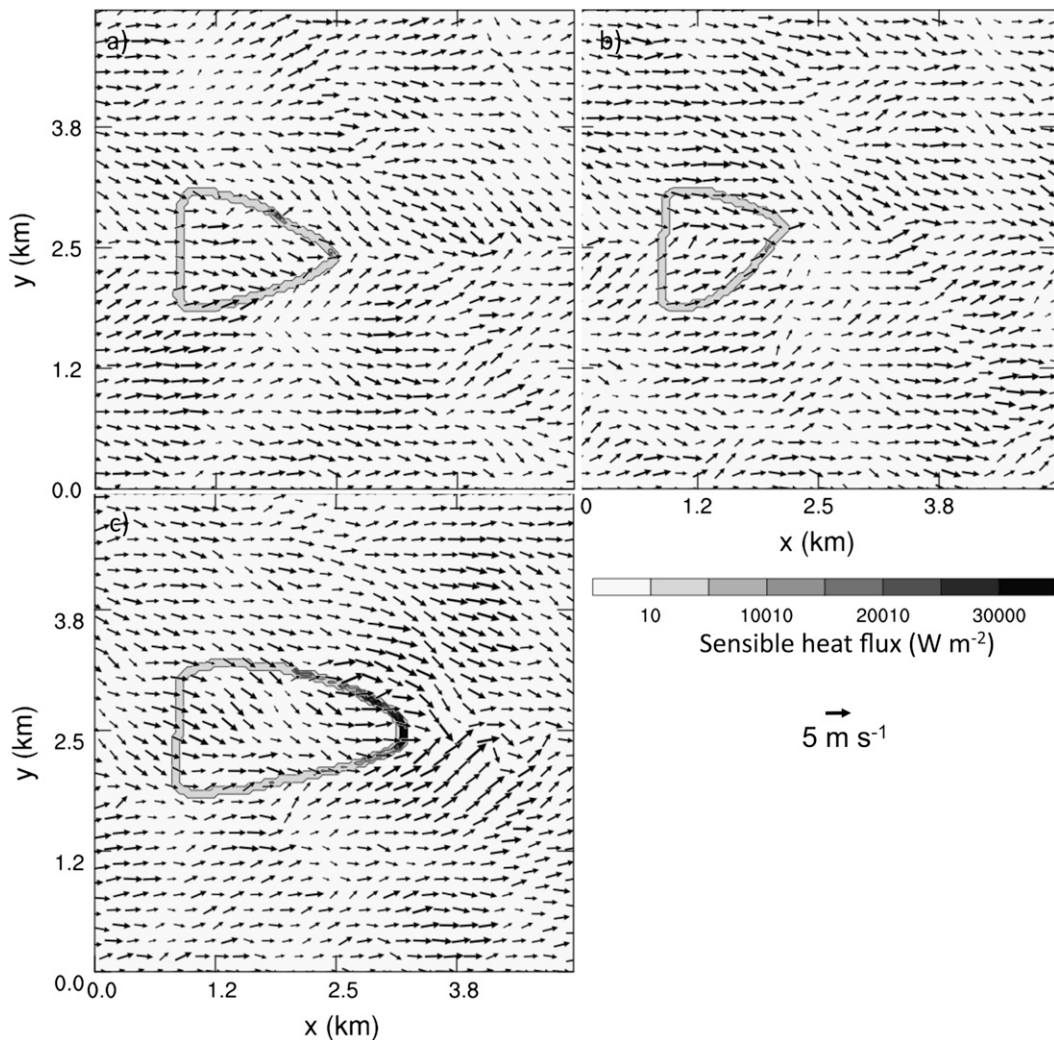


FIG. 8. Three simulations of a fire at 2.5 h (2 h after ignition) in varying fuel loads including (a) the control experiment at 0.167 kg m^{-2} , (b) one-half of the fuel load of (a), and (c) 2 times the fuel load of (a). Contours indicate sensible heat flux, and vectors indicate near-surface wind speeds.

The stronger vertical velocities produced by higher fuel loads may have other important consequences in fire effects such as scorch height but, as implemented here, the impact on fire rate of spread was relatively limited. Different fuel loads similarly had a minor effect on the fire line's shape. Also, the burning depth was not affected because, in the algorithms applied, the fuel mass lost in each time step was calculated [Eq. (6)] as a percentage of the original fuel load and, other fuel properties being equal, the fire released more heat for larger loads but did not take longer to burn out.

d. Sensitivity to wind speed

It has been widely held that wind is one of the most important and most rapidly changing environmental factors affecting fire behavior and that higher wind

speeds produce faster fire spread rates over a wide range of wind speeds and fuels. Yet, a more detailed inspection shows that the mechanisms through which this occurs are not clear and probably depend on the fire-propagation mechanism at work (Morvan et al. 2002). In the context of kinematic uncoupled models, much of the discussion hinges upon the exponent to which the wind speed is raised in relationships [e.g., Eqs. (1), (4), and (5)] between the horizontal wind speed and the resulting fire rate of spread. Weise and Biging (1997), Fendell and Wolff (2001), and Sandberg et al. (2007) compiled relationships from laboratory experiments and field experiments on small fires, in which the exponent ranged from 0.4 to 2.7, implying that a doubling of the wind speed could cause the fire's rate of spread to more than double. Carrier et al. (1991) posed relationships of rate

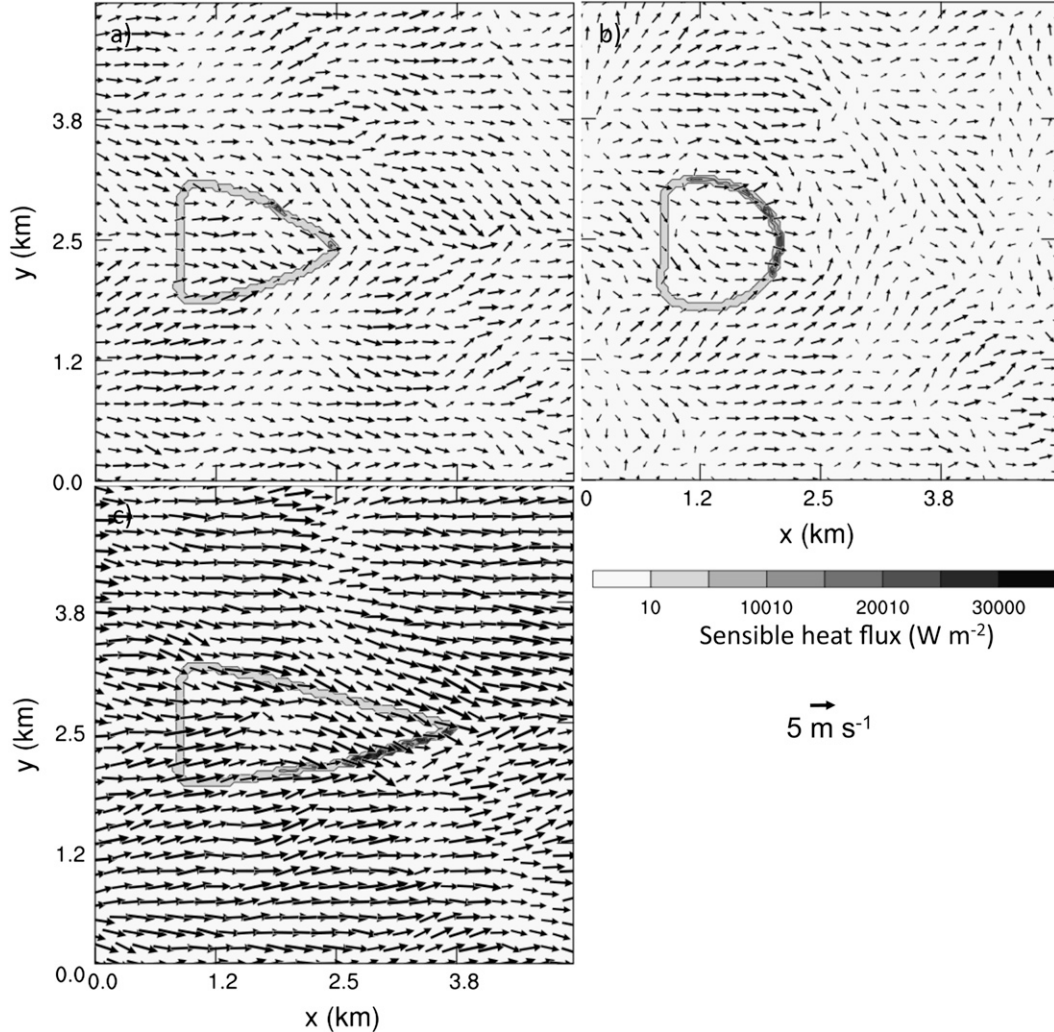


FIG. 9. Three simulations of a fire in varying wind speeds at 2 h, all from the left, including (a) the control experiment at 2.5 m s^{-1} , (b) one-half of the wind speed of (a), and (c) 2 times the wind speed of (a). Contours indicate sensible heat flux, and vectors indicate near-surface wind speeds.

of spread as a function of the square root of the ratio of the wind speed to fuel load and used experimental results by Wolff et al. (1991) to include the impact of other parameters. Simulations with models employing a more detailed representation of fire processes also provide a point of reference. For example, Mell et al. (2007)'s coupled CFD–fire model produced a linear increase from 0.4 to 1.5 m s^{-1} in the spread rate of the leading edge of a grass fire as ambient winds at 2 m above ground were varied from 1 to 5 m s^{-1} . In similar experiments, Linn and Cunningham's (2005) coupled CFD–fire model simulations produced an increase in spread rate from 0.27 to 1.37 m s^{-1} as ambient winds were increased from 1 to 6 m s^{-1} .

We tested the model's sensitivity to varying the 2.5 m s^{-1} wind speed of the control experiment (Fig. 9a)

by halving it (experiment WSLo, Fig. 9b) and doubling it (experiment WSHi, Fig. 9c). This range of wind speeds, a factor-of-4 difference between the weakest and strongest nonzero wind experiments, affects not only the ambient winds but also the turbulent eddies. For a given imposed heat source, as the ambient wind speed increases, the shear velocity and Obukhov length (the characteristic height of the sublayer of dynamic turbulence) increase and the nature of the turbulence changes (Arya 1988). Our range of wind speeds spanned the convective boundary layer regime, our regime of interest. Increasing further the imposed wind speed would drive the turbulence regime toward a neutral boundary layer dominated by horizontal roll vortices, much different than the other experiments and outside our interest. The difference in flow structures, statistics, and turbulent kinetic energy

budget distributions between shear and buoyancy-driven boundary layers is described by Moeng and Sullivan (1994).

As expected, with all other parameters held constant across the simulations, stronger wind speeds led to a faster-moving fire: halving wind velocity reduced spread rate by one-fifth, and doubling wind velocity increased spread rate by four-fifths. Because of atmospheric coupling, higher wind speeds led to a narrower simulated fire in the crosswind direction (Fig. 9), however. The fire perimeter remained symmetric even though the relative locations of the fire line and surface convergence/divergence of turbulent eddies created transient horizontal sensible heat-flux asymmetries along the fire line, which implied transient perturbations in buoyancy, vertical velocity, and vertical vorticity. The burning depth over which a minimal sensible heat flux occurred remained similar for all three experiments, as did the peak sensible heat fluxes.

A rise in ambient wind speed not only increases the rate at which the fire line contacts fresh fuel along its perimeter but also alters the nondimensional convective Froude number F_c , a parameter characterizing the relative importance of streamwise momentum to the plume's buoyancy forcing. Byram (1959) suggested that a value of $F_c = 1$ be considered the critical value separating subcritical ($F_c < 1$) buoyancy-dominated plume-driven fires from supercritical ($F_c > 1$) wind-driven fires. In calculating F_c with the method of Clark et al. (1996b), F_c varied from 0.3 (WSLo), through 0.5 (Control), to 0.6 (WSHi) across this range of wind speeds and remained in the subcritical buoyancy-driven regime.

e. Sensitivity to fuel moisture

Because of the energy consumed to vaporize water absorbed by dead fuel and held between the cells in live fuels, increased fuel moisture is expected to reduce a fire's rate of spread, although there is still no fundamental explanation for how fuel moisture affects the chemical reaction rates during combustion or decreases the rate of spread (Rothermel 1972; Sandberg et al. 2007). Although observations in some ecosystems showed fire to spread in fuels with high moisture content, Rothermel's (1972) model truncates a fire's estimated rate of spread at fuel moisture contents higher than some critical value (the moisture content of extinction)—a feature that has generated some critique (e.g., Weise and Biging 1997). This truncation results from Rothermel's (1972) generalized curve fit, which was developed to capture a moisture-damping effect observed in laboratory experiments in which fire spread through the top layer of pine needles packed on a weighing table, an effect that may not be applicable to other fuel types.

Three experiments vary the fuel moisture, where fuel moisture content (%) is expressed as 100 times the mass of water (kg) per kilogram of oven-dry fuel weight. We examined the sensitivity of WRF to fuel moisture contents of 5.5% in the control experiment (Fig. 10a), low (2.75%) fuel moisture in experiment FMLo (Fig. 10b), and a higher fuel moisture (11%) in experiment FMHi (Fig. 10c), each of which is less than the presumed moisture content of extinction (12%) for short grass. FMLo produced a slightly faster-spreading fire with a rate of spread of 0.34 m s^{-1} and a higher peak sensible heat flux of 31 kW m^{-2} in the heading region, as compared with the Control experiment with a rate of spread of 0.22 m s^{-1} and peak heat flux of 25 kW m^{-2} . FMHi, with its fuel moisture content very close to short grass's moisture content of extinction, produced a very slowly moving fire with rate of spread of 0.044 m s^{-1} and low sensible heat flux of 4 kW m^{-2} . As a result, it did not release enough heat to focus the winds into an obvious heading region. The burning depth was unaffected by this parameter and, in all three experiments, the fire perimeter maintained the universal shape.

5. Conclusions

The results demonstrated that line fires simulated using WRF with WRF-Fire generally evolved into a naturally observed bowed shape that results from fire-atmosphere feedbacks determining the flow in and near fires, but even in conditions with idealized wind and uniform fuels the flow structure near the head and flanks of the simulated fires differed dramatically and produced asymmetrically developing fires. The coupled model reproduced the known sensitivity of fires to changes in initial conditions, including differences in fire shapes, heading-region intensity, and burning depth among grass, shrub, and forest-litter fuel types. It also reproduced the observed tendency of dry, heavy fuels in strong winds to lead to faster-moving fires, although the effect of fuel load is largely to generate stronger plumes, with small impact on the spread rate. These faster fires were generally determined to be a consequence of how the heat and moisture released by the fire focused the fire's energy in the heading region, shaping the fire plume and consequently, through convergence into the base of the plume, the near-fire winds. This shows that dynamic models have the potential to add illumination beyond what kinematic models offer because they connect the fire behavior through physically consistent relationships with fire effects such as smoke production, plume strength, and smoke transport height. The introduction of shear-generated and convectively generated boundary layer turbulence to simulations in general confirmed

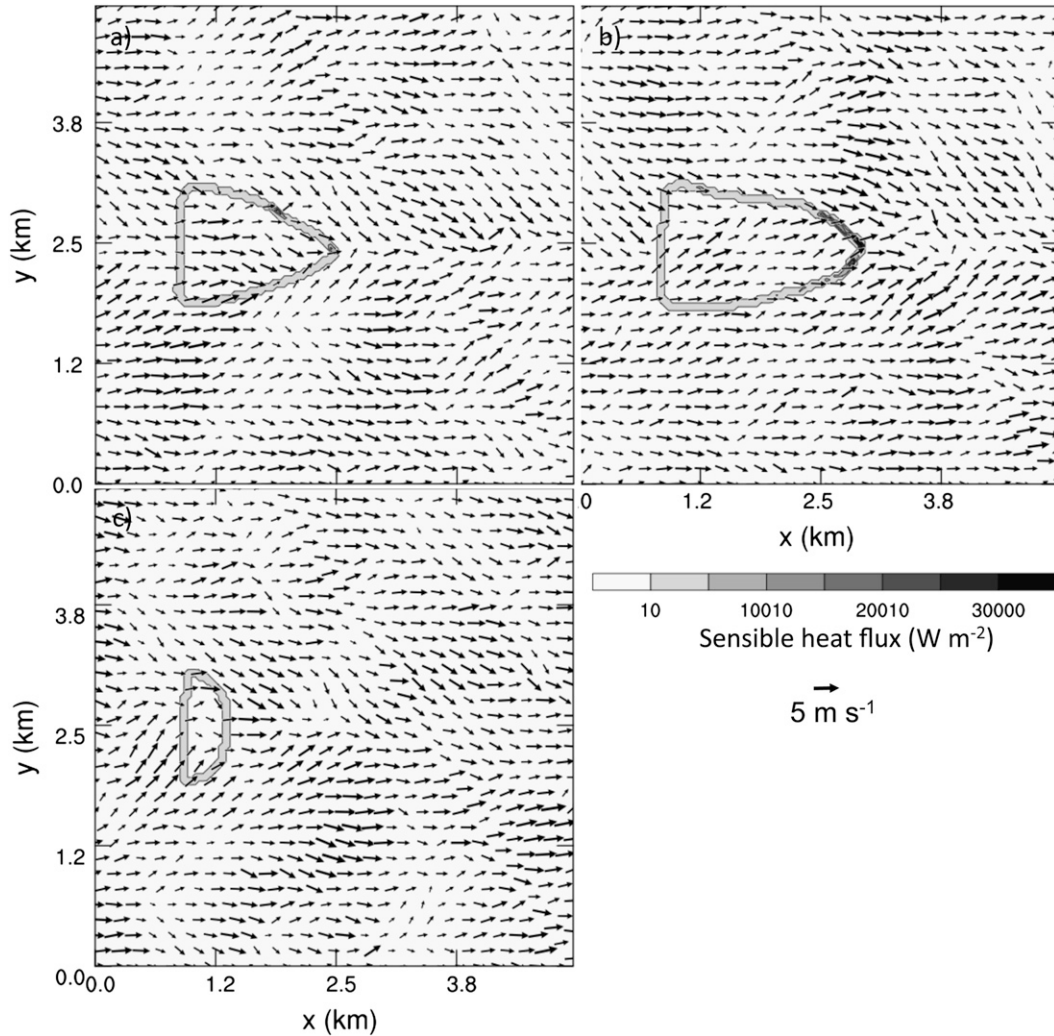


FIG. 10. Three simulations of a fire in varying fuel moisture conditions at 2 h, including (a) the control experiment at 5.5%, (b) relatively low fuel moisture (2.75%) for fuel model 1, and (c) relatively high fuel moisture (11%) as compared with fuel model 1's 12% moisture content for extinction. Contours indicate sensible heat flux, and vectors indicate near-surface wind speeds.

that the fire heading region, flanks, and backing region and the accompanying fire-influenced wind pattern were stable to small perturbations, which appeared as transient fluctuations along the flanks [shown in earlier simulations by Clark et al. (2004) to result in fire whirls]. Larger perturbations, caused, for example, by heavy fuel loads, could in certain combinations of other parameters cause unstable growth of the fire.

6. Discussion

This work focused on testing the sensitivity of the coupled model, WRF with WRF-Fire, to factors for which expected behavior is known from previously accumulated knowledge within the wildland fire community, either

through measurements in similar conditions or through prior model results when the behavior has not been observed in experimental fires. In assessing our results, we note that it is important that the complexity of the physics be scale-commensurate for the phenomena being studied. Whereas many fire processes occur at spatial scales smaller than tens of meters, coupled weather–fire models aim to capture the interactions and phenomena resulting from fires at scales that are resolvable by a range of atmospheric models. At these grid lengths of tens of meters, flames, the details of combustion processes, and the mixing between flammable gases and surrounding oxygen are not resolved. Instead, the fire acts as a temporally and spatially varying source of buoyancy and water vapor in the lowest 100 m above the

earth's surface, which may span one or several vertical grid levels. Previous simulations (Clark et al. 1996a,b, 2004; Coen 2005) united a fire module with a cloud-scale atmospheric model where horizontal grid spacing ranged from 20 m to 1 km. In applying a subset of that fire behavior physics package within the WRF model run in LES mode, this work examined whether the gross response of simulated wildland fires to different idealized environmental conditions could be reproduced in a model designed primarily for mesoscale modeling studies. Later studies will build on the results of this work, which examined the effect of four parameters in simple atmospheric and fuel conditions and will test it against data on experimental fires and landscape-scale wildland fires.

One of the most critical factors for successful modeling of fire behavior with coupled weather–fire models is accurate calculation of the near-surface atmospheric wind, this being the sole input from the atmospheric model. Although it is possible to simulate atmospheric flows at many spatial and temporal scales with WRF, it is well known that the simulated atmospheric motions are not scale independent; neither are the effects of fire feedbacks on atmospheric motions. There are different implications at each end of the spectrum of possible grid spatial scales.

Using WRF in LES mode and allowing a convective boundary layer to form before igniting a fire produced fluctuations in the wind and turbulent structures that interacted with the motions produced by the fire. With this type of fire module, the fluctuations bias the fire simulations toward faster fire growth. This effect is apparent in the simulations of Sun et al. (2009), who concluded that turbulence led to faster-spreading fires. (In fact, the semiempirical algorithms that relate rate of spread to environmental wind speed may need to be recalibrated for LES use at these scales.) The issue is that, while a wind fluctuation forward at the flaming front may advance the fire in a jump through contact with fuels ahead of the fire, a wind fluctuation backward into the flaming front produces no counterbalancing effect in the model; once fuel is ignited, it continues to burn. Our simulations with stronger turbulent fluctuations generated by an imposed 200 W m^{-2} sensible heat flux (not shown) produced unstably accelerating, asymmetrically growing fires that spread at angles up to 45° from the ambient downwind direction. Although wildland fires are certainly turbulent fluid-dynamical flows and many phenomena undoubtedly arise from dynamic exchanges, the ability of wind shifts created by the fire to amplify unstably through feedbacks with the fire suggest that caution should be applied in interpreting model results.

At the large-scale end of the spectrum of spatial scales that might be used in wildland fire simulations, WRF's

strength lies in its design and application as a mesoscale model, in which boundary layer fluxes are parameterized with one of many boundary layer schemes, using horizontal grid spacing of 2–10 km and vertical grid spacing of hundreds of meters. At this coarse scale, turbulent motions and the effects of small topographic features are not captured. Although the fire module is not sensitive to fire gridcell resolution, the simulated atmospheric flow and associated fire feedbacks are. The resolved mesoscale velocities represent a grid-volume average, upon which the 10–20-m-wide fire-line heat fluxes may not be distinguishable; here we note that a requirement for the success of dynamic coupled weather–fire models is that the fire alters the atmospheric winds enough to shape the fire line. The mismatch in scales among the 10–20-m fire-line burning depth, the heat release in the lowest 50 m of the atmosphere, and mesoscale-model spatial scales of 2–10 km may be difficult to overcome in practice. There are also known biases in mesoscale model-generated wind speeds [an example is the topographic overestimations on hills and underestimates in valleys in WRF noted by Jimenez and Dudhia (2012)] that complicate simulations at the coarser end of coupled weather–fire modeling.

Acknowledgments. This material is based upon work supported by the National Science Foundation under Awards 0324910, 0421498, and 0835598. The National Center for Atmospheric Research (NCAR) is sponsored by the National Science Foundation. Any opinions, findings, and conclusions or recommendations expressed in this material are those of the authors and do not necessarily reflect the views of the National Science Foundation. Marques Cameron was supported by the University Corporation for Atmospheric Research's Significant Opportunities in Atmospheric Research and Science (SOARS) program. WRF, including the WRF-Fire physics module, is available as public domain software at <http://www.wrf-model.org>. Contributions to WRF-Fire came from numerous individuals at NCAR, the U. S. Department of Agriculture Forest Service, the Australian Bureau of Meteorology, and the University of Colorado at Denver. We thank Peter Sullivan for helpful discussions during this work. We thank Alan Norton of NCAR's Computational & Information Systems Laboratory (CISL) for help with visualizations using VAPOR.

REFERENCES

- Albini, F. A., 1976: Estimating wildfire behavior and effects. USDA Forest Service General Tech. Rep. INT-30, 92 pp.
—, 1993: Dynamics and modeling of vegetation fires: Observations. *Fire in the Environment: The Ecological, Atmospheric,*

- and Climatic Importance of Vegetation Fires*, P. J. Crutzen and J. G. Goldammer, Eds., John Wiley and Sons, 39–52.
- , 1994: Program BURNUP: A simulation model of the burning of large woody natural fuels. Montana State University Mechanical Engineering Dept. USDA Forest Service Research Grant INT-92754-GR Final Rep., 113 pp.
- , J. K. Brown, E. D. Reinhardt, and R. D. Ottmar, 1995: Calibration of a large fuel burnout model. *Int. J. Wildland Fire*, **5**, 173–192.
- Alexander, M. E., B. J. Stocks, B. M. Wotton, and R. A. Lanoville, 1998: An example of multi-faceted wildland fire research: The International Crown Fire Modelling Experiment. *Proc. III Int. Conf. Forest Fire Research /14th Conf. Fire and Forest Meteorology*, Coimbra, Portugal, University of Coimbra, 83–112.
- Anderson, H. E., 1982: Aids to determining fuel models for estimating fire behavior. USDA Forest Service, Intermountain Forest and Range Experiment Station General Tech. Rep. INT-122, 22 pp. [Available online at http://www.fs.fed.us/rm/pubs_int/int_gtr122.pdf.]
- Andrews, P. L., C. D. Bevins, and R. C. Seli, 2008: BehavePlus fire modeling system, version 4.0: User's guide. USDA Forest Service, Rocky Mountain Research Station, General Tech. Rep. RMRS-GTR-106WWW, 132 pp.
- Arya, S. P., 1988: *Introduction to Micrometeorology*. Academic Press, 307 pp.
- Butler, B. W., and M. B. Dickinson, 2010: Tree injury and mortality in fires: Developing process-based models. *Fire Ecol.*, **6**, 55–79.
- Byram, G. M., 1959: Forest fire behavior. *Forest Fires: Control and Use*, K. P. Davis, Ed. McGraw-Hill, 90–123.
- Carrier, G. F., F. E. Fendell, and M. F. Wolff, 1991: Wind-aided firespread across arrays of discrete fuel elements. I. Theory. *Combust. Sci. Technol.*, **75**, 31–51.
- Cheney, N. P., and J. S. Gould, 1995: Fire growth in grassland fuels. *Int. J. Wildland Fire*, **5**, 237–247.
- , —, and W. R. Catchpole, 1993: The influence of fuel, weather and fire shape variables on fire-spread in grasslands. *Int. J. Wildland Fire*, **3**, 31–44.
- Clark, T. L., M. A. Jenkins, J. Coen, and D. Packham, 1996a: A coupled atmosphere–fire model: Convective feedback on fire-line dynamics. *J. Appl. Meteor.*, **35**, 875–901.
- , —, —, and —, 1996b: A coupled atmosphere–fire model: Role of the convective Froude number and dynamic fingering at the fireline. *Int. J. Wildland Fire*, **6**, 177–190.
- , J. Coen, and D. Latham, 2004: Description of a coupled atmosphere–fire model. *Int. J. Wildland Fire*, **13**, 49–64.
- Clements, C. B., and Coauthors, 2007: Observing the dynamics of wildland grass fires: FireFlux: A field validation experiment. *Bull. Amer. Meteor. Soc.*, **88**, 1369–1382.
- Coen, J. L., 2005: Simulation of the Big Elk Fire using coupled atmosphere–fire modeling. *Int. J. Wildland Fire*, **14**, 49–59.
- , 2011: Some new basics of fire behavior. *Fire Manage. Today*, **71**, 37–42.
- , and P. J. Riggan, 2010: Landscape-scale wildland fire modeling: Research & applications. *Proc. Australasian Fire Authorities Council and Bushfire Cooperative Research Centre Conf.*, Darwin, Northern Territories, Australia, Australasian Fire Authorities Council, CD-ROM, 11 pp. [Available from the Australasian Fire and Emergency Service Authorities Council, Level 5, 340 Albert St., East Melbourne, VIC 3002, Australia.]
- , S. Mahalingam, and J. W. Daily, 2004: Infrared imagery of crown-fire dynamics during FROSTFIRE. *J. Appl. Meteor.*, **43**, 1241–1259.
- Deardorff, J. W., 1980: Stratocumulus-capped mixed layers derived from a three-dimensional model. *Bound.-Layer Meteor.*, **18**, 495–527.
- Dupuy, J. L., 1995: Slope and fuel load effects on fire behavior: Laboratory experiments in pine needles fuel beds. *Int. J. Wildland Fire*, **5**, 153–164.
- Fendell, F. E., and M. F. Wolff, 2001: Wind-aided fire spread. *Forest Fires: Behavior and Ecological Effects*, E. A. Johnson and K. Miyanishi, Eds., Academic Press, 171–221.
- Finney, M. A., 1998: FARSITE: Fire Area Simulator—Model development and evaluation. USDA Forest Service, Rocky Mountain Station, Research Paper RMRS-RP-4, 47 pp. [Available online at <http://nature.berkeley.edu/stephens-lab/fireareaall.pdf>.]
- Frankman, D. J., 2009: Radiation and convection heat transfer in wildland fire environments. Ph.D. dissertation, Brigham Young University, 232 pp. [Available online at <http://contentdm.lib.byu.edu/cdm/singleitem/collection/ETD/id/1838>.]
- Hinzman, L. D., M. Fukuda, D. V. Sandberg, F. S. Chapin III, and D. Dash, 2003: FROSTFIRE: An experimental approach to predicting the climate feedbacks from the changing boreal fire regime. *J. Geophys. Res.*, **108**, 8153, doi:10.1029/2001JD000415.
- Jimenez, P. A., and J. Dudhia, 2012: Improving the representation of resolved and unresolved topographic effects on surface wind in the WRF model. *J. Appl. Meteor. Climatol.*, **51**, 300–316.
- Kremens, R. L., A. M. S. Smith, and M. Dickinson, 2010: Fire metrology: Current and future directions in physics-based measurements. *Fire Ecol.*, **6**, 13–35.
- Linn, R., and P. Cunningham, 2005: Numerical simulations of grass fires using a coupled atmosphere–fire model: Basic fire behavior and dependence on wind speed. *J. Geophys. Res.*, **110**, D13107, doi:10.1029/2004JD005597.
- , J. Reisner, J. Colman, and J. Winterkamp, 2002: Studying wildfire behavior using FIRETEC. *Int. J. Wildland Fire*, **11**, 233–246.
- Mallet, V., D. E. Keyes, and F. E. Fendell, 2009: Modeling wildland fire propagation with level set methods. *Comput. Math. Appl.*, **57**, 1089–1101.
- Mandel, J., J. D. Beezley, J. Coen, and M. Kim, 2009: Data assimilation for wildland fires: Ensemble Kalman filters in coupled atmosphere–surface models. *IEEE Control Syst. Mag.*, **29** (3), 47–65.
- , —, and A. K. Kochanski, 2011: Coupled atmosphere–wildland fire modeling with WRF 3.3 and SFIRE 2011. *Geosci. Model Dev.*, **4**, 591–610.
- McAlpine, R. S., 1995: Testing the effect of fuel consumption on fire spread rate. *Int. J. Wildland Fire*, **5**, 143–152.
- McArthur, A. G., 1969: The Tasmanian bushfires of 7th February, 1967, and associated fire behavior characteristics. *Proc. Mass Fire Symposium, Canberra, Australia, 1969*, Maribyrnong, VIC, Australia, Defence Standards Laboratories, 23 pp.
- Mell, W., M. A. Jenkins, J. Gould, and P. Cheney, 2007: A physics-based approach to modeling grassland fires. *Int. J. Wildland Fire*, **16**, 1–22.
- Moeng, C.-H., and P. P. Sullivan, 1994: A comparison of shear- and buoyancy-driven planetary boundary layer flows. *J. Atmos. Sci.*, **51**, 999–1022.
- , J. Dudhia, J. Klemp, and P. Sullivan, 2007: Examining two-way grid nesting for large eddy simulation of the PBL using the WRF model. *Mon. Wea. Rev.*, **135**, 2295–2311.

- Morvan, D., V. Tauleigne, and J. L. Dupuy, 2002: Flame geometry and surface to crown fire transition during the propagation of a line fire through a Mediterranean shrub. *Proc. Fourth Int. Conf. on Forest Fire Research*, Coimbra, Portugal, Association for the Development of Industrial Aerodynamics, 10 pp. [Available online at <http://www.eufirelab.org/toolbox2/library/upload/236.pdf>.]
- National Wildfire Coordinating Group, 1994: Introduction to wildland fire behavior S-190. National Interagency Fire Center NFES 180, 66 pp.
- Noble, I. R., G. A. V. Bary, and A. M. Gill, 1980: McArthur's fire danger meters expressed as equations. *Aust. J. Ecol.*, **5**, 201–203.
- Osher, S. J., and J. A. Sethian, 1988: Front propagating with curvature-dependent speed: Algorithms based on Hamilton-Jacobi formulations. *J. Comput. Phys.*, **79**, 12–49.
- Palmer, T., 1981: Large fire winds, gases, and smoke. *Atmos. Environ.*, **15**, 2079–2090.
- Patton, E. G., and J. L. Coen, 2004: WRF-Fire: A coupled atmosphere-fire module for WRF. Preprints, *5th WRF/14th MM5 Users' Workshop*, Boulder, CO, National Center for Atmospheric Research, 221–223. [Available online at http://www.mmm.ucar.edu/mm5/workshop/ws04/Session9/Patton_Edward.pdf.]
- Potter, B., and B. Butler, 2009: Using wind models to more effectively manage wildfire. *Fire Manage. Today*, **69**, 40–46.
- Pyne, S. J., P. L. Andrews, and R. D. Laven, 1996: *Introduction to Wildland Fire*. 2nd ed. John Wiley and Sons, 769 pp.
- Rehm, R. G., and R. J. McDermott, 2009: Fire-front propagation using the level set method. NIST Tech. Note 1611, 12 pp. [Available online at http://www2.bfrl.nist.gov/userpages/wmell/PUBLIC/TALKS_PAPERS/Rehm_McDermott_fire_level_set_NIST_TN_1611_09.pdf.]
- Richards, G. D., 1990: An elliptical growth model of forest fire fronts and its numerical solution. *Int. J. Numer. Methods Eng.*, **30**, 1163–1179.
- Riggan, P. J., L. G. Wolden, R. G. Cissel, and J. Coen, 2010: Remote sensing fire and fuels in southern California. *Proc. Third Fire Behavior and Fuels Conf.*, Spokane, WA, International Association of Wildland Fire, 14 pp. [Available online at http://www.fs.fed.us/psw/publications/riggan/psw_2010_riggan002.pdf.]
- Rothermel, R. C., 1972: A mathematical model for predicting fire spread in wildland fuels. USDA Forest Service, Intermountain Forest and Range Experiment Station, Research Paper INT-115, 40 pp. [Available online at <http://www.treesearch.fs.fed.us/pubs/32533>.]
- Sandberg, D. V., C. L. Riccardi, and M. D. Schaaf, 2007: Reformulation of Rothermel's wildland fire behaviour model for heterogeneous fuelbeds. *Can. J. For. Res.*, **37**, 2438–2455.
- Schmidt, H., and U. Schumann, 1989: Coherent structure of the convective boundary layer derived from large-eddy simulations. *J. Fluid Mech.*, **200**, 511–562.
- Sethian, J. A., 1996: *Level Set Methods: Evolving Interfaces in Computational Geometry, Fluid Mechanics, Computer Vision, and Materials Science*. Cambridge University Press, 237 pp.
- Skamarock, W. C., J. B. Klemp, J. Dudhia, D. O. Gill, D. M. Barker, W. Wang, and J. G. Powers, 2005: A description of the Advanced Research WRF version 2. NCAR Tech. Note TN-468+STR, 88 pp.
- Sun, R., S. K. Krueger, M. A. Jenkins, M. A. Zulauf, and J. J. Charney, 2009: The importance of fire atmosphere coupling and boundary-layer turbulence to wildfire spread. *Int. J. Wildland Fire*, **18**, 50–60.
- Tymstra, C., R. W. Bryce, B. M. Wotton, S. W. Taylor, and O. B. Armitage, 2010: Development and structure of Prometheus, the Canadian wildland fire growth simulation model. Natural Resources Canada Information Rep. NOR-X-417, 102 pp. [Available online at http://firegrowthmodel.ca/download/Prometheus_Information_Report_NOR-X-417_2010.pdf.]
- Van Wagner, C. E., 1989: Prediction of crown fire behavior in conifer stands. *Proc. 10th Conf. Fire & Forest Meteorology*, Ottawa, ON, Canada, Forestry Canada, 207–211.
- Weise, D. R., and G. S. Biging, 1997: A qualitative comparison of fire spread models incorporating wind and slope effects. *For. Sci.*, **43**, 170–180.
- Wolff, M. F., G. F. Carrier, and F. E. Fendell, 1991: Wind-aided firespread across arrays of discrete fuel elements. II. Experiment. *Combust. Sci. Technol.*, **77**, 261–289.
- Yedinak, K. M., B. Lamb, and J. L. Coen, 2010: Sensitivity analyses and application of WRF-Fire. *Proc. Third Fire Behavior and Fuels Conf.*, Spokane, WA, International Association of Wildland Fire, CD-ROM, 7 pp. [Available from the International Association of Wildland Fire, 1418 Washburn St., Missoula, MT 59801.]